

By HONGLIANG ZHANG[®], Member IEEE, BOYA DI[®], Member IEEE, KAIGUI BIAN[®], Senior Member IEEE, ZHU HAN[®], Fellow IEEE, H. VINCENT POOR[®], Life Fellow IEEE, AND LINGYANG SONG[®], Fellow IEEE

ABSTRACT | In future cellular systems, wireless localization and sensing functions will be built-in for specific applications, e.g., navigation, transportation, and healthcare, and to support flexible and seamless connectivity. Driven by this trend, the need for fine-resolution sensing solutions and centimeter-level localization accuracy arises, while the accuracy of current wireless systems is limited by the quality of the propagation environment. Recently, with the development of new materials, reconfigurable intelligent surfaces (RISs) provide an opportunity to reshape and control the electromagnetic characteristics of the environment, which can be utilized to improve the performance of wireless sensing and localization. In this tutorial, we will first review the background and motivation for utilizing wireless signals for sensing and localization. Next, we will introduce how to incorporate RIS into applications of sensing and localization, including key challenges and enabling techniques, and then, some case studies will be presented. Finally, future research directions will also be discussed.

KEYWORDS | Implementation; localization; reconfigurable intelligent surfaces (RISs); wireless sensing.

Manuscript received September 30, 2021; revised January 20, 2022; accepted April 17, 2022. This work was supported in part by the National Key Research and Development Project of China under Grant 2020YFB1807100; in part by the National Natural Science Foundation of China under Grant 61829101, Grant 61941101, and Grant 62032003; in part by the Beijing Natural Science Foundation under Grant 4222005 and Grant L212027; in part by the State Key Laboratory of Advanced Optical Communication Systems Networks, China; and in part by the U.S. National Science Foundation under Grant CNS-2107216 and Grant EARS-1839818. (Corresponding author: Lingyang Song.)

Hongliang Zhang is with the School of Electronics, Peking University, Beijing 100871, China, and also with the Department of Electrical and Computer Engineering, Princeton University, Princeton, NJ 08544 USA.

Boya Di and Lingyang Song are with the School of Electronics, Peking University, Beijing 100871, China (e-mail: lingyang.song@pku.edu.cn). Kaigui Bian is with the School of Computer Science, Peking University, Beijing 100871, China.

Zhu Han is with the Department of Electrical and Computer Engineering, University of Houston, Houston, TX 77004 USA, and also with the Department of Computer Science and Engineering, Kyung Hee University, Seoul 446-701, South Korea.

H. Vincent Poor is with the Department of Electrical and Computer Engineering, Princeton University, Princeton, NJ 08544 USA.

Digital Object Identifier 10.1109/JPROC.2022.3169771

I. INTRODUCTION

A. Sensing and Localization in Future Cellular **Systems: Basic Requirements**

Driven by a wide range of emerging applications such as automated vehicles and robots, future wireless networks will be required to enable high-resolution environmental awareness in order to fulfill interactions between the digital and physical worlds. This can be achieved by sensing and localization functions in wireless networks. In other words, a device in the wireless network should have the ability to know its location as well as detect the presence of objects (including their shapes, locations, and speeds of movement) in the operating environment using transmitted or received radio signals [1].

In this regard, the fifth-generation (5G) networks already provide possibilities for accurate localization and

0018-9219 © 2022 IEEE. Personal use is permitted, but republication/redistribution requires IEEE permission. See https://www.ieee.org/publications/rights/index.html for more information.

sensing services with their larger bandwidth and massive antenna arrays, and the sixth generation (6G) should continue this trend [2]. As defined by the 3GPP, 5G needs to satisfy a level of accuracy of less than 1 m for more than 95% of the network area [3], and 6G is envisioned to achieve subcentimeter accuracy [4]. These tolerances will require the evolution of radio frequency (RF) sensing and localization techniques to support such high accuracy.

B. Motivation: Why Reconfigurable Intelligent Surfaces?

Current wireless systems highly depend on the quality of the propagation environment, which is conventionally modeled as an exogenous entity that can only be adapted to but not controlled. This is challenged by future wireless systems that integrate communication, sensing, and localization functions into one single platform. It is thus desirable that the wireless environment should be treated as part of the network design [5].

With the development of metamaterials, this new design of wireless networks can be facilitated by an emerging technology, which is referred to as reconfigurable intelligent surfaces (RISs) [6]. RISs are comprised of thin layers of metamaterials capable of shaping wireless signals that impinge upon the surface such that propagation environments can be customized to fulfill specific system requirements [7]. This can be achieved by controlling the phases and amplitudes of impinging radio signals through nearly passive and low-cost elements embedded in an RIS [8]. As a result, the RIS can provide favorable propagation conditions to improve sensing and localization accuracy. In particular, the RIS can manipulate the signals from different targets or locations to be more distinguishable, which makes it easier for the receiver to detect targets or estimate their locations.

C. Use Cases

Wireless sensing and localization have a variety of applications in our daily lives, such as indoor navigation, transportation, healthcare, and security [9]. In the following, we will elaborate on these application scenarios to show the importance of accurate and ubiquitous sensing and localization.

- 1) Indoor navigation: Indoor navigation is a common use case in shopping malls, factories, and airports, and it necessitates accurate localization for the user. Different from outdoor scenarios, indoor localization suffers from severe line-of-sight (LoS) blockage that will significantly degrade the accuracy [10]. This can be alleviated by deploying an RIS on a wall to provide virtual LoS links, which is particularly important in industrial Internet-of-Things applications [11], e.g., factory robots.
- 2) Intelligent transportation: Autonomous driving [12] and vehicle-to-everything (V2X) communications [13] are envisioned as two potential ways to realize intelligent transportation. For autonomous driving, it is critical for a vehicle to be able to build a real-time

- map and detect its environment, which requires accurate distances among vehicles or between the vehicle and surrounding obstacles for safe operation. For V2X communications, the measurement of the velocity can help predict the location of a vehicle, which will further improve the communication performance. With the RIS attached to buildings and billboards, localization and sensing accuracy can be further enhanced, thus improving the safety and efficiency of transportation systems.
- 3) Healthcare: Physical activity recognition for healthcare, such as fall detection, is an important application of wireless sensing due to its contact-free nature, i.e., users do not need to carry devices or modify their daily routines [14]. For these applications, reliability and accuracy are the most important concerns, which are highly dependent on the quality of channel conditions [15]. By deploying RISs, the wireless propagation environment can be customized to alleviate these issues.
- 4) Security: RF sensing can also be used for security applications, e.g., theft monitoring [16]. These applications require extremely high sensing accuracy, as missed detections might cause serious consequences. However, the accuracy of traditional sensing methods is limited by channel conditions. The accuracy can be further improved by deploying an RIS for favorable channel conditions.

D. Contribution and Organization

In this article, we aim to provide a tutorial overview on enabling RF sensing and localization using RISs, by reviewing the state-of-the-art results in the literature, presenting new ideas to solve the main challenges for sensing and localization accuracy improvement, and introducing a hardware prototype implementation. Moreover, we identify promising research directions related to RIS-aided RF sensing and localization with the hope of motivating future work. It is worth noting that, to the authors' best knowledge, this article is the first tutorial paper to address the issues in RF sensing and localization applications with RISs.

The rest of this article is organized as follows. We present the fundamentals in Section II, including the principle of RF sensing and localization, as well as the basics of RISs and corresponding signal models. Sections 1 and 2 elaborate on the enabling technologies for RIS-aided sensing and localization applications, respectively. In Section V, we introduce how to implement such a system and show some important experimental results. In Section VI, we outline possible future directions. Finally, we conclude this article in Section VII.

II. FUNDAMENTALS OF RF SENSING AND LOCALIZATION WITH RISS

In this section, we provide some preliminary background on RF sensing and localization as well as RIS technology. In Section II-A, we first introduce how to use RF signals to

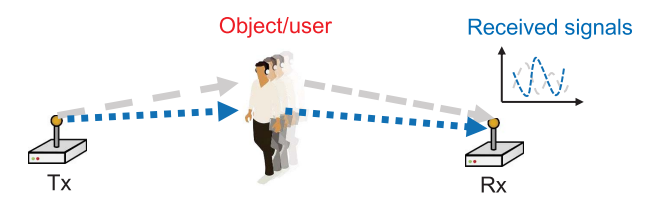


Fig. 1. Illustration of sensing using wireless signals.

realize sensing and localization. In Section II-C, we then present some basics of RISs, and finally, in Section II-D, we present the RF signal models in an RIS-aided wireless network.

A. Working Principle

The basic idea of utilizing RF signals for sensing and localization applications is to extract information from wireless signals. However, there are still some differences between sensing and localization applications, which will be elaborated in the following.

1) RF Sensing: The working principle underlying RF sensing is that the presence of objects will cause changes in wireless signals, which results in a variation of certain properties of received signals [17]. As a result, we can detect the existence of objects from the variation of received signals. A typical RF sensing system is shown in Fig. 1. There is a transmitter (Tx) and a receiver (Rx), and the Rx will analyze the received signals to recognize the movement of users or the existence of objects.

2) RF Localization: Localization is based on the extraction of location-related information, such as distance or arrival angle, from received signals [18]. An example of an RF localization system is shown in Fig. 2. There are several anchor nodes (ANs) whose locations are known to transmit/receive wireless signals to help locate the user's position. In such a system, the user will acquire the distances to these ANs from received signals and derive its position accordingly. In order to obtain a unique position, it requires at least three ANs. In the sensing systems, objects are located between the Tx and the Rx so that the Rx can detect the changes caused by the objects. Alternatively, the Rx in a localization system can be held by the user when it is the user who wants to know its own position.

B. Measurement Metrics

To measure the changes or extract location-related information, there are various metrics corresponding to different signal properties. The commonly used metrics are reviewed in the following.

1) Received Signal Strength: Received signal strength (RSS) indicates how the wireless channel influences the amplitude of wireless signals on average, which is an easily acquired metric. In general, the RSS at the Rx with the

distance to the Tx being d can be derived through the lognormal distance path loss model [19], i.e.,

$$P(d) = P_T - 10\alpha \log d + e_{RSS},\tag{1}$$

where P(d) is the received RSS measured in decibels (dB), P_T is the transmitted energy, α is the path loss exponent, and $e_{\rm RSS}$ is the noise in the RSS measurement. For sensing applications, the existence of objects within the sensing area will cause significant signal attenuation, i.e., α will be different, which leads to the variation of RSS measurements. For localization applications, the distance between the user and the AN can be obtained from the RSS.

2) Channel State Information: Channel state information (CSI) captures the frequency response of the wireless channel. CSI can be obtained by comparing the known transmitted signals in the packet preamble or pilot carriers to the received signals. Different from RSS which only provides the amplitude information, CSI consists of a set of complex values, including both amplitude and phase information, which correspond to multiple orthogonal frequency-division multiplexing (OFDM) subcarriers. Therefore, CSI allows fine-grained channel estimation and can be mathematically expressed as

$$\boldsymbol{h} = [h_1, \dots, h_N]^T, \tag{2}$$

where N is the number of subcarriers and $h_i = a_i e^{j\psi_i}$, with a_i being the amplitude of the CSI obtained at the ith subcarrier and ψ_i being the corresponding phase. In general, CSI is more commonly used in sensing applications since

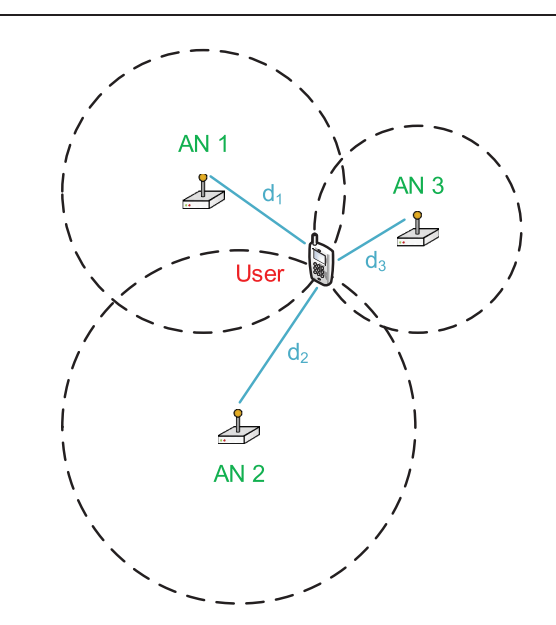


Fig. 2. Illustration of localization using wireless signals.

it can provide more information to capture the movements of objects [20].

3) Time of Flight: Time of flight (ToF) is the time span between instants when a signal is transmitted and received. With the ToF measurement, we can obtain the distance d between the Rx and the Tx as [21]

$$c \cdot \tau_{\text{ToF}} = d + e_{\text{ToF}},\tag{3}$$

where c is the speed of light, τ_{ToF} is the derived ToF for the transmitted signals, and e_{ToF} is the noise for the ToF measurement. In general, the measurement of ToF can be categorized into the following two types.

 Direct measurements using OFDM signals: Since OFDM is the most commonly used radio waveform, it is important to introduce how to obtain the ToF using OFDM symbols. A received discrete-time OFDM symbol after removing the cyclic prefix (CP) can be expressed as [22]

$$y_n = e^{\frac{j2\pi\rho n}{N}} \sum_{l=1}^{L} h_l x_{lT_s - \tau_l} + \omega_n,$$
 (4)

where n denotes the subcarrier index, x_n is the timedomain OFDM waveform sampled at the rate of $1/T_s$, in which T_s equals the symbol duration divided by the number of subcarriers N, h_l is the channel coefficient of the lth path with delay τ_l , and L is the total number of paths. ρ is the residual carrier frequency offset after frequency synchronization and ξ_n is additive white Gaussian noise. Assume that $\tau_1 \leq \cdots \leq \tau_L$, and τ_1 is the ToF that we defined before. Existing methods to estimate the ToF are mainly the MUSIC algorithm [23], the SAGE algorithm [24], and the MPLR algorithm [22]. We take the MPLR algorithm as an example here. The basic idea of the MPLR algorithm is to maximize the peak-to-leaking ratio of the estimated channel impulse response (CIR), which is a function of the delay. As a result, we can obtain the ToF using optimization tools.

2) Frequency-modulated Continuous-wave (FMCW) radars: FMCW radars [25] provide another method to obtain the ToF. These radars transmit continuous waves, which allows transmitted signals to stay within a constant power envelop, thus reducing the power and the cost for signal processing. The working principle of FMCW is shown in Fig. 3. The Tx sends a chirp with linearly increasing frequency, and the Rx compares the received and transmitted signals at any time instant to calculate the frequency difference f_d . Given the slope of the linear chirp η , the ToF can be directly obtained as $\tau_{ToF} = (f_d/\eta)$. Compared to the direct measurement method, FWCW radars do not require wide bandwidth or a high sampling rate,

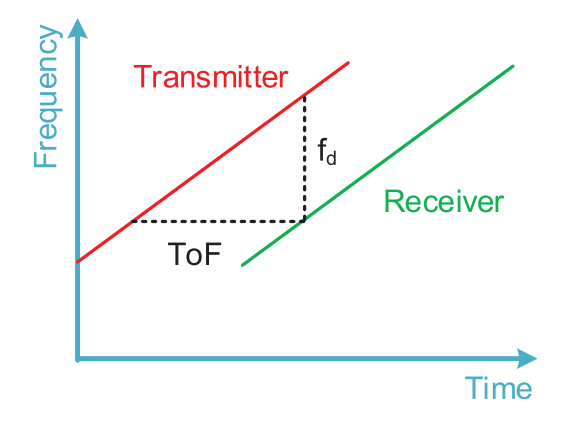


Fig. 3. Working principle of FMCW.

which is more suitable for systems having relatively narrow bandwidths.

4) Doppler Shift: Doppler shift is a property of wireless signals caused by relative movements that can be utilized to capture the movements of sensing targets or locate users over the observed frequency [26]. For example, in sensing applications, a positive Doppler shift implies that the sensing target is moving toward the Rx, while a negative value indicates that the target is moving away from the Rx. Assuming that the sensing target moves at speed v in the direction of ϕ toward the Rx, the resulting Doppler shift is expressed as

$$\Delta f = \frac{2v\cos(\phi)}{c}f,\tag{5}$$

where f is the center frequency of the transmitted signal.

5) Angle of Arrival: Sensing and localization can also be facilitated by the detection of angle of arrival (AoA), which is also referred to as the direction of arrival (DoA). In sensing applications, by tracking the AoA, the Rx can tell whether the signals are reflected from the sensing area. In localization applications, the AoA-based localization method as shown in Fig. 4 only requires two ANs, while the distance-based localization method as shown in Fig. 2 requires three ANs.

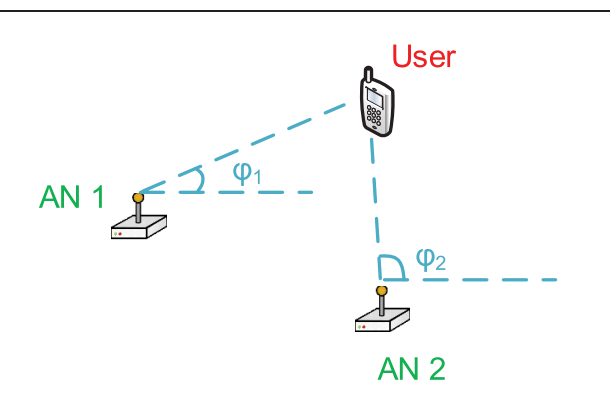


Fig. 4. AoA-based localization method.

Fig. 5. Different types of RISs: (a) reflective type, (b) refractive type, and (c) hybrid type.

Assume that the user's and the ith AN's locations are $\boldsymbol{u} = [u_x, u_y]^T$ and $\boldsymbol{a}_i = [a_x^i, a_y^i]^T$, respectively. Then, the measured AoA can be written as [18]

$$\varphi_i = \arctan\left(\frac{u_y - a_y^i}{u_x - a_x^i}\right) + e_{AoA}^i,$$
 (6)

where e_{AoA}^i is the measurement error. Therefore, we can infer the location of the user through the measured AoAs using (6). To measure the AOAs, the Rx should be equipped with antenna arrays or directional antennas with spatial resolution capabilities.

C. RIS Basics

RISs are thin layers of electromagnetic (EM) metamaterials capable of shaping radio waves that impinge upon them in such a way that the wireless environment can be customized to fulfill specific system requirements [27]. According to the implementation, RISs can be categorized into three types [30].

- 1) Reflective Type: In this type, an RIS only reflects incident signals toward the users on the same side of the base station (BS), as shown in Fig. 5(a). In the literature, this type of RIS is also referred to as an intelligent reflecting surface (IRS) [31].
- 2) Refractive Type: In this type, incident signals will penetrate the RIS and be refracted toward users on the opposite side of the BS, as shown in Fig. 5(b).
- 3) Hybrid Type: This type of RIS enables a dual function of reflection and refraction [32]. In other words, the incident signals are split into two parts: one part is refracted and the other is reflected, as shown in Fig. 5(c). This type of RIS is also referred to as an intelligent omni-surface (IOS) [33].

Although an RIS is composed of multiple layers, each layer might vary for different types. As shown in Fig. 6, we will take the reflective RIS as an example to show how the RIS is built. A reflective RIS consists of the following three lavers.

1) The outer layer is a 2-D array of RIS elements, which can directly interact with incident signals.

- 2) The middle layer is a copper plate that can prevent signal energy leakage.
- 3) The inner layer is a printed circuit connecting to the RIS controller, which can control the phase shifts of the RIS elements.

Each RIS element is a low-cost subwavelength programmable metamaterial particle, whose working frequency can vary from sub-6 GHz to terahertz (THz) [28]. When an EM wave impinges on the RIS element, a current will be induced by the EM wave, and this induced current will cause EM radiation based on the permittivity ϵ and permeability μ of the RIS. This is how the RIS element controls the wireless signals. An example of a metamaterial particle is given in Fig. 7. As illustrated in this figure, positive intrinsic negative (p-i-n) diodes are embedded in each element. By controlling the biasing voltage through the via hole, the p-i-n diode can be switched between "ON" and "OFF" states. The "ON" and "OFF" states of the p-i-n diodes lead to different values of ϵ and μ . As a result, this element will have a different response to incident signals by imposing different phase shifts and amplitudes [29].

To illustrate this behavior, we first consider the response of one RIS element. We define the additional phase shift introduced by the RIS as θ . The value of θ can be continuous if the RIS is implemented with varactors, while θ has finite values if it is implemented with p-i-n diodes. Assuming that B p-i-n diodes are used in the

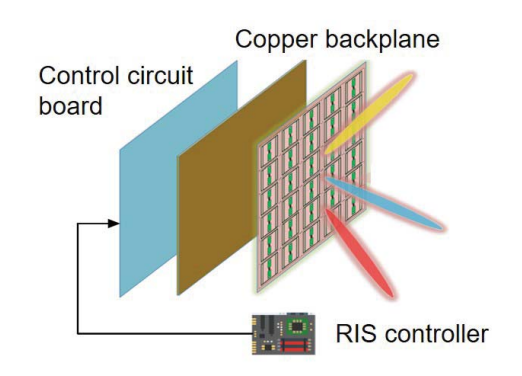


Fig. 6. Components of a reflective RIS.

Zhang et al.: Toward Ubiquitous Sensing and Localization With Reconfigurable Intelligent Surfaces

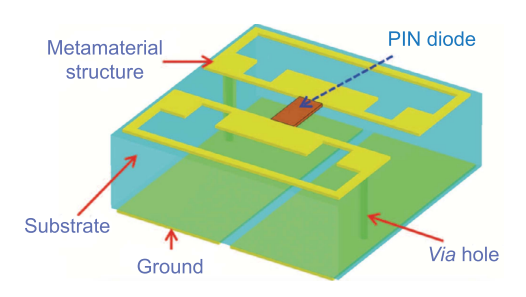


Fig. 7. Example of a programmable metamaterial particle.

RIS, we have K possible phase shifts with $K \leq 2^B$, which can be expressed as $\mathcal{K} = \{0,\ldots,2n\pi/K,\ldots,2(K-1)\pi/K\}, 1 \leq n \leq K-1$ [34]. In the following, since the RIS can be divided into three types, we will show how these three types of RISs respond to the incident signals.

1) Reflective Type: According to [35], the response of an RIS element can be written as

$$\gamma = \Gamma e^{-j\theta},\tag{7}$$

where j is the imaginary unit, i.e., $j^2 = -1$. Here, $\Gamma \in [0, 1]$ is the amplitude of the RIS response, where $\Gamma = 1$ indicates that the incident signals are fully reflected, while $\Gamma\,=\,0$ implies that the incident signals are fully absorbed. The response is determined by the tuning impedance of the equivalent circuit for each element and mutual impedances (if mutual coupling cannot be ignored) at the ports of the RIS, and it is generally influenced by azimuth and elevation angles for incident and reflected signals, i.e., ϕ^A , ψ^A , ϕ^D , and ψ^D , as shown in Fig. 8(a). Moreover, Γ and θ are usually sensitive to the working frequency. The reflection coefficients will vary when the same RIS receives signals at different frequencies. However, the RIS will be designed to operate over a predefined band where the phase shift and amplitude can be regarded as unchanged over the considered bandwidth.

- *2) Refractive Type:* As shown in Fig. 8(b), similar to the reflective type, the response of a refractive RIS element can also be expressed in the form of (7). The only difference is that the incident signals fully penetrate the RIS element when $\Gamma=1$.
- 3) Hybrid Type: The hybrid RIS element has the functions of both reflection and refraction. Therefore, the RIS will first split the energy of incident signals into two parts: one for refractive signals and the other for reflective signals. To quantify the energy separation, we introduce a metric $\beta \in [0, +\infty)$, which is the power ratio of reflected signals to refracted signals [36]. Therefore, we assume that there is no energy leakage and that the response of a hybrid RIS element to reflected and refracted signals can also be expressed in the form of (7), where the phase shifts to reflected and refracted signals might be different.

Therefore, the reflective and refractive responses can be expressed as

$$\gamma_{\text{refl}} = \sqrt{\frac{\beta}{1+\beta}} \Gamma_{\text{refl}} e^{-j\theta_{\text{refl}}},$$
 (8)

$$\gamma_{\text{refr}} = \sqrt{\frac{1}{1+\beta}} \Gamma_{\text{refr}} e^{-j\theta_{\text{refr}}}, \tag{9}$$

where $\Gamma_{\rm refl}$ and $\Gamma_{\rm refr}$ are the reflection and refraction, respectively, and $\theta_{\rm refl}$ and $\theta_{\rm refr}$ are the phase shifts for reflection and refraction, respectively. It is worth noting that the hybrid type will be reduced to the reflective type with $\beta=+\infty$ and the refractive type with $\beta=0$.

For the rest of this article, we take the reflective-type RISs as examples, and the term "RIS" typically refers to the reflective RIS for brevity. The same idea can also be applied to refractive or hybrid RISs.

D. RF Signal Modeling With RISs

With an RIS, a single-user communication system is shown in Fig. 9. In the following, we will introduce how to model the signals in an RIS-aided communication system. We will start with a single subcarrier and then extend the modeling to an OFDM system.

- 1) Single Subcarrier: Over the *n*th subcarrier, the received signals are composed of three components: the LoS component, the reflection component, and the multipath component, as elaborated in the following.
- a) LoS component: This indicates the direct signal path from the Tx to the Rx. Denote $h_{\rm los}$ as the channel gain for the LoS component. Based on [26], $h_{\rm los}$ can be expressed as

$$h_{\rm los}^n = \frac{\lambda}{4\pi} \cdot \frac{\sqrt{g_T g_R} \cdot e^{-j2\pi d_{\rm los}/\lambda_n}}{d_{\rm los}},\tag{10}$$

where λ_n is the wavelength of the signals transmitted on the nth subcarrier, g_T and g_R denote antenna gains of the Tx and the Rx, respectively, and $d_{\rm los}$ is the distance between the Tx and the Rx.

b)Reflection component: This is the LoS paths from the Tx to the Rx via the reflections of the RIS, where each RIS element corresponds to one reflection path. Assume that the RIS consists of M elements and define h_m as the gain of the reflection path via the mth RIS element. Based on [37] and [38], h_m can be written as

$$h_m^n = \frac{\lambda \sqrt{g_T g_R} \gamma_m e^{-j2\pi \left(d_m^T + d_m^R\right)/\lambda_n}}{8\pi^{3/2} d_m^T d_m^R},\tag{11}$$

where γ_m is the mth RIS element's response as defined in (7) and d_m^T and d_m^R are the distances from the mth RIS element to the Tx and Rx, respectively. Note that the multipath component will also be reflected by the RIS. However, the channel gain of the reflection of the multipath component is much less than

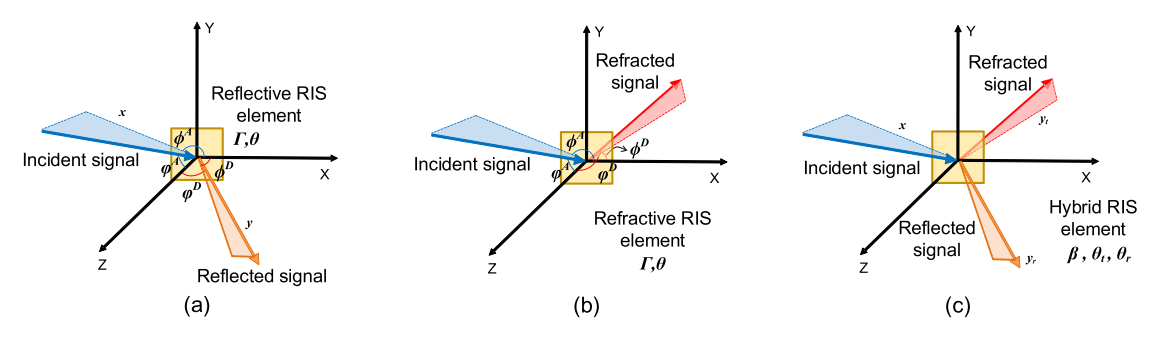


Fig. 8. Response for an RIS element of three types: (a) reflective type, (b) refractive type, and (c) hybrid type.

that of the LoS reflection component, and thus, the reflection of the multipath component is neglected here

c) Multipath component: The environmental scattering paths account for the signal paths between the Tx and the Rx, which involve complex scattering from the surrounding environment. We denote $h_{\mathrm{sc}}^n \in \mathbb{C}$ as the equivalent gain of all the environmental scattering paths.

Based on the above notation, the received signals over the *n*th subcarrier can be expressed as

$$y_n = \left(h_{\text{los}}^n + \sum_{m=1}^M h_m^n + h_{\text{sc}}^n\right) x_n + \omega_n,\tag{12}$$

where x_n denotes the transmitted symbol over the nth subcarrier and ω_n is the noise, in which $\omega_n \sim \mathcal{CN}(0, \sigma^2)$ with σ^2 being the noise power.

2) OFDM Systems: Let $\mathbf{x} = [x_1, \dots, x_N]^T$ be an OFDM symbol. The OFDM symbol is first transformed into the time domain via an N-point inverse discrete Fourier transform (IDFT) and then is appended by a CP At the Rx, after removing the CP and performing an N-point discrete Fourier transform (DFT), the equivalent baseband signals

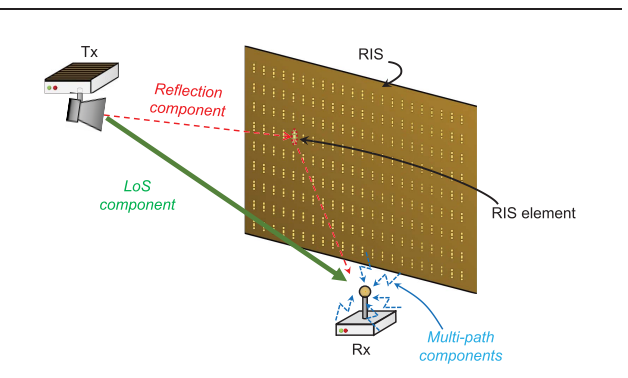


Fig. 9. Single-user communication system with an RIS.

in the frequency domain at the Rx can be expressed as

$$y = X(h_{\text{los}} + h_{\text{reflect}} + h_{\text{sc}}) + \omega,$$
 (13)

where $\boldsymbol{y} = [y_1, \dots, y_N]^T$ is the received OFDM symbol, $\boldsymbol{X} = \operatorname{diag}(\boldsymbol{x})$ is the diagonal matrix of OFDM symbol $\boldsymbol{x}, \ \boldsymbol{h}_{\operatorname{los}} = [h_{\operatorname{los}}^1, \dots, h_{\operatorname{los}}^N]^T$ is the channel response of the LoS component, $\boldsymbol{h}_{\operatorname{reflect}} = [\sum_{m=1}^M h_m^1, \dots, \sum_{m=1}^M h_m^N]^T$ is the channel response of the reflection component, $\boldsymbol{h}_{\operatorname{sc}} = [h_{\operatorname{sc}}^1, \dots, h_{\operatorname{sc}}^N]^T$ is the channel response of the multipath component, and $\boldsymbol{\omega} = [\omega_1, \dots, \omega_N]^T$ is the noise. According to (13), we can adjust the phase shifts of the RIS to customize the received signals for a certain system requirement.

III. RIS-AIDED SENSING

In this section, we will introduce RIS-aided RF sensing applications. In traditional RF sensing problems, one needs to optimize the decision function to map the received signals to sensing results. However, the use of the RIS introduces two unique challenges in system design. First, RIS configurations need to be carefully designed to provide a favorable wireless propagation environment for sensing applications. Different from the design for communications, which aims to maximize the received signal-tonoise ratio (SNR), the RIS configuration design for sensing applications is to enhance the differences of signals in the presence of different sensing targets, which makes it easier for the Rx to distinguish them. Second, as the RIS can manipulate the received signals, the decision function design is highly coupled with the RIS configurations, which makes the design of the decision function challenging.

In general, RF sensing techniques can be divided into two types according to the used RF signals. One is to utilize commodity signals, such as Wi-Fi and cellular signals, which we refer to as MetaSensing. The other one is to use customized signals, i.e., radar, which is referred to as MetaRadar. In contrast to the first type, radar sensing can adjust the transmitted waveform and thus can have better sensing accuracy. However, it requires an extra pair of transceivers for signal transmission and reception, which

is more likely to be used in accuracy-sensitive applications, such as autonomous driving. In Section III-A and III-B, we will present the details of MetaSensing and MetaRadar systems, respectively, to address the above challenges.

A. MetaSensing: Sensing With Commodity Signals

A general MetaSensing system with commodity signals is shown in Fig. 10. In such a system, there exists a pair of a Tx and Rx, an RIS, and a target space where the objects (or human bodies) are located. Here, the Tx and Rx are commercial devices, for example, Wi-Fi access points (APs) and smartphones. The target space is a cubical region that is discretized into Q uniform space blocks. The transmitted signals are customized by the RIS before entering into the target space. The customized signals are further reflected by the objects in the target space and received by the Rx unit. As a result, the Rx can map the received signals, including LoS and reflected links, to the sensing results.

To synchronize the RIS, the Tx, and the Rx, a sensing protocol is proposed [39]. In the protocol, the timeline is divided into cycles, where the Tx, the Rx, and the RIS are operated in a synchronized and periodic manner. As shown in Fig. 11, each cycle consists of four phases.

- 1) *Synchronization phase:* The Tx transmits a synchronization signal to the RIS and to the Rx, which identifies the start time of a cycle.
- 2) Calibration phase: As the received LoS path contains no information about the target space, we generate a reference signal in this phase, which will be used to subtract the LoS path. To be specific, the RIS is set to a default configuration, and the Rx records the received reference signal y₀.
- 3) Data collection phase: The timeline in this phase is equally divided into frames. During this phase, the Tx continuously transmits the RF signal, while the RIS changes its configuration at the end of each frame, as shown in Fig. 11. The received signals are denoted by y. To remove the LoS path, the received signals in these frames are subtracted by the reference signal. In particular, the differences between the received signals and the reference signals constitute a mea-

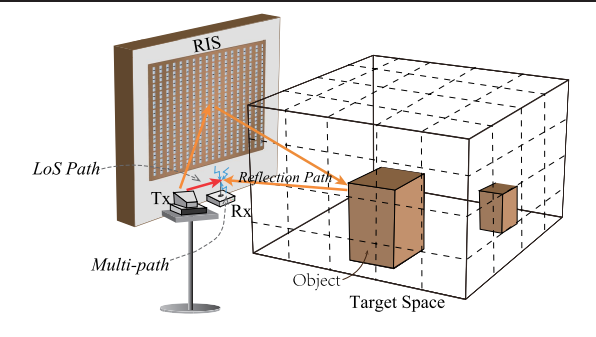


Fig. 10. Illustration for MetaSensing systems.



Fig. 11. Cycle of the sensing protocol.

surement vector \hat{y} , where

$$\hat{\boldsymbol{y}} = \boldsymbol{y} - \boldsymbol{y}_0 = \tilde{\boldsymbol{\Gamma}} \boldsymbol{\nu} \boldsymbol{x} + \tilde{\boldsymbol{\omega}}. \tag{14}$$

Here, y_0 is a reference vector where all the elements are the reference signal y_0 obtained in the previous phase, and x is the transmitted signal. ν is the reflection coefficients of these space blocks, which can be used to determine the existence of the target on each block. $\tilde{\omega}$ is the noise difference between the received signals and the reference signal, which is still Gaussian. $\tilde{\Gamma}$ is the difference between the channel gains under the RIS configurations selected in this phase and that under the default configuration.

4) *Data processing phase:* The Rx maps the measurement vectors obtained in the data collection phase to the sensing results using a decision function.

To improve the sensing performance, the configuration of the RIS and the decision function at the Rx needs to be optimized. In the following, we will introduce two use cases. The first one is a known object set, where at least partial information about the targets is known. The second one is an unknown object set, where no prior information about the targets is given.

1) Case I: A Known Object Set: For a known object set, we take posture recognition as an example, where the set of possible postures \mathcal{I} is known [40], and we want to figure out what the posture is from the received signals. To quantify the sensing performance, we define the weighted cost caused by false recognition under the decision function L as the average false recognition cost, where

$$\Psi_L = \sum_{i,i' \in \mathcal{I}, i \neq i'} p_i \chi_{i,i'} \int \Pr(\hat{\boldsymbol{y}}_i | \boldsymbol{\nu}_i) L_{i'}(\hat{\boldsymbol{y}}_i) d\hat{\boldsymbol{y}}_i.$$
 (15)

Here, p_i is the prior probability of the ith human posture, ν_i is the reflection coefficient vector of the ith posture, $\chi_{i,i'}$ is the cost of recognizing the ith posture as the i'th one, $\Pr(\hat{y}_i|\nu_i)$ is the probability of the measurement vector being \hat{y}_i given ν_i , and $L_{i'}(\hat{y}_i)$ is the probability that the Rx will map the measurement vector \hat{y}_i to the i'th posture.

a) RIS configuration optimization: This problem is to minimize the average false recognition cost by optimizing the configuration matrix, which is involved in $\tilde{\Gamma}$. Moreover,

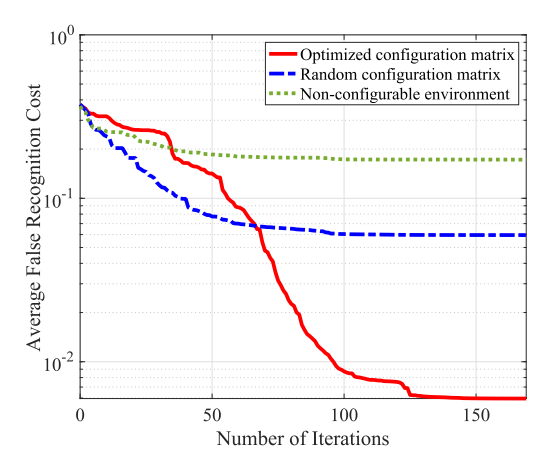


Fig. 12. Average false recognition cost versus the number of training iterations with ten cycles.

the optimized configuration matrix for specific coefficient vectors may be sensitive to subtle changes in the postures. Therefore, we will reformulate the objective for a general posture recognition scenario.

Based on the observations that most of the space blocks are empty and thus have zero reflection coefficients, and for the blocks where the human body is situated, only those that contain the surfaces of the human body with specific angles can reflect the incident signals toward the Rx and thus have nonzero reflection coefficients, the reflection vector for the target space ν is sparse and can be reconstructed using compressive sensing. According to the theory in [41], to reduce the loss of reconstruction for sparse target signals, we can minimize the average mutual coherence of $\tilde{\Gamma}$, which is defined as

$$\mu(\tilde{\Gamma}) = \frac{1}{Q(Q-1)} \sum_{q,q',q \neq q'} \frac{|\tilde{\gamma}_q^T \tilde{\gamma}_{q'}|}{\|\tilde{\gamma}_q\|_2 \|\tilde{\gamma}_{q'}\|_2}, \quad (16)$$

where $ilde{\gamma}_q$ is the qth column of $ilde{\Gamma}$ and $\|\cdot\|_2$ denotes the

b) Decision function optimization: The objective of this problem is to minimize the cost by optimizing the decision function L. To solve this problem efficiently, we employ a neural network to approximate the decision function. The input is the measurement vector \hat{y} and the output is the probability distribution over all postures in \mathcal{I} . This neural network can be trained by the backpropagation algorithm.

Fig. 12 shows the average false recognition cost versus the number of training iterations for the neural network in the decision function optimization for a dataset collected from our prototype (see [40] for details). Here, the costs of true and false recognition are set to 0 and 1, respectively, i.e., $\chi_{i,i'} = 0$ if i = i', and otherwise, $\chi_{i,i'} = 1$. It can be observed that the converged value of the average false recognition cost with the proposed RIS configuration optimization method is less than 10% of that obtained with a random RIS configuration. Moreover, compared to the nonreconfigurable environment case, i.e., without the

assistance of the RIS, we can observe that the capability of the RIS to customize the environment helps the RF sensing system to significantly reduce the average false recognition cost.

2) Case II: An Unknown Object Set: For an unknown object set, we have no information about the number and shape of possible objects, and we aim to obtain a 3-D sketch of the objects in a given space from the received signals. As a result, we cannot use the false recognition cost to quantify the sensing accuracy. Instead, we use the cross-entropy loss Ψ to measure the sensing accuracy [42]. To be specific, the cross-entropy loss is generally used to calculate the difference between the measured probability distribution and the ground-truth distribution over the target space, where

$$\Psi = -\mathbb{E}_{\nu} \left[\sum_{q=1}^{Q} p_q(\nu) \ln(\hat{p}_q) + (1 - p_q(\nu)) \ln(1 - \hat{p}_q) \right].$$
(17)

Here, $p_a(\nu)$ is a binary variable indicating the object's existence in the qth space block. In other words, $p_q(\nu) = 0$ if $|\nu| = 0$; otherwise, $p_q(\nu) = 1$. \hat{p}_q is the estimated result obtained from measurement vector \hat{y} using a decision function $f(\hat{\boldsymbol{y}})$.

This problem aims to minimize the cross-entropy loss by optimizing the configuration matrix that is involved in Γ . As we do not have any information about the objects, the sparsity assumption may not hold in this case. Therefore, the compressive sensing method cannot be applied anymore. As each RIS element has a finite number of phase shifts, the optimization problem can be reformulated as a Markov decision process (MDP).

- 1) State: The state of the environment includes the index of the current frame, the index of the RIS element to adjust its phase shift, and the RIS configuration matrix, including the configurations of the RIS over all the frames in the data collection phase. The state is called a terminal state when the phase shifts of all the RIS elements over all the frames are determined.
- 2) Action: In each state, the RIS element indicated by the index adjusts its phase shift under the current configuration of the RIS.
- 3) Transition: A nonterminal state will transit to the state where the index of the RIS element increases by 1. Moreover, if the last RIS element selects its phase shift in the current state, then, in the next state, the index of the frame will increase by 1 and the index of the RIS element will be reset to 1. During the transition, the RIS configuration matrix is updated according to the phase shift adjusted by the RIS element in the current state.
- 4) Reward: The reward is defined as the negative crossentropy loss of the mapping of the received signals given the configuration determined in the terminal state. If the terminal state has not been reached, the reward for the state transition is set to be zero.

Zhang et al.: Toward Ubiquitous Sensing and Localization With Reconfigurable Intelligent Surfaces

Ground Truth Proposed PRPG SensNet + PolicyNet		SensNet + rand control matrix	SensNet w/o opt linear decoder + PolicyNet	Only opt linear decoder
Z	Z	Z	Z	2
x y	x y	x y	x y	x y
Z	Z	Z	Z	Z
x y	x y	x y	x y	x y
x y	x	x y	x y	x

Fig. 13. Sensing result comparisons for different shapes of objects.

Under such an MDP framework, we propose a deep reinforcement learning algorithm to jointly optimize the RIS configuration and decision function. To be specific, the reinforcement learning algorithm consists of two phases as follows, and these two phases proceed iteratively until it converges. Please refer to [39] for more details. Based on the results obtained after the convergence, we can further perform semantic recognition and segmentation to obtain meaningful representations of the objects [43].

a) RIS configuration optimization phase: The RIS starts from an initial state and adopts a policy function to select actions in each state until it reaches the terminal state. As the set of feasible actions is large, we use a neural network, called the policy network, to approximate the policy function, where the inputs are the states, while the output is the probability distribution of the actions. The policy network is trained to maximize the accumulated rewards.

b) Decision function optimization phase: Similarly, the decision function is also approximated by a neural network, called the sensing network. The inputs are the received signals \hat{y} under the configurations obtained by the policy network, and the output is the sensing result. The sensing network is trained to minimize the cross entropy defined in (17).

In Fig. 13, we show the ground truths and the sensing results for different shapes of objects in a typical example (details can be found in [39]). The schemes for these results are: 1) ground truths for comparison; 2) the proposed scheme where both sensing and policy networks are used; 3) the sensing network is used while a random RIS configuration is adopted; 4) the policy network is utilized, while a model-aided decoder contained in the sensing

network is removed; and 5) only the model-aided decoder is used. From the comparison, we can observe that the proposed algorithm outperforms other benchmark algorithms to a large extent and that both sensing and policy networks contribute to improving the sensing accuracy. Moreover, we can observe that the proposed algorithm obtains accurate sensing results despite the different shapes of the objects.

It is worth pointing out that Case I is a special case of Case II. In other words, the methods in Case II can also be used for Case I. However, the complexity of the method proposed for Case I is typically lower than that for Case II since we can use the prior information to reduce the feasible set.

B. MetaRadar: Sensing With Radar Signals

A multitarget detection scenario using a MetaRadar is shown in Fig. 14. The MetaRadar is composed of a Tx, an Rx, a multiple-input multiple-output (MIMO) antenna array connected with the Tx and Rx, and an RIS [44]. By deploying an RIS in the radar system, we can improve the overall channel conditions between the antenna array and sensing targets. The MetaRadar has two modes, i.e., transmission and reception modes. In the transmission mode, the Tx first generates signals according to designed waveforms and then radiates the signals through the MIMO antenna array toward the targets via both direct and reflection paths, as shown in Fig. 14(a). Then, the MetaRadar system switches to the reception mode, where the antenna array receives the echo signals reflected by the targets. The received signals will be delivered to the Rx in order to detect and locate targets.

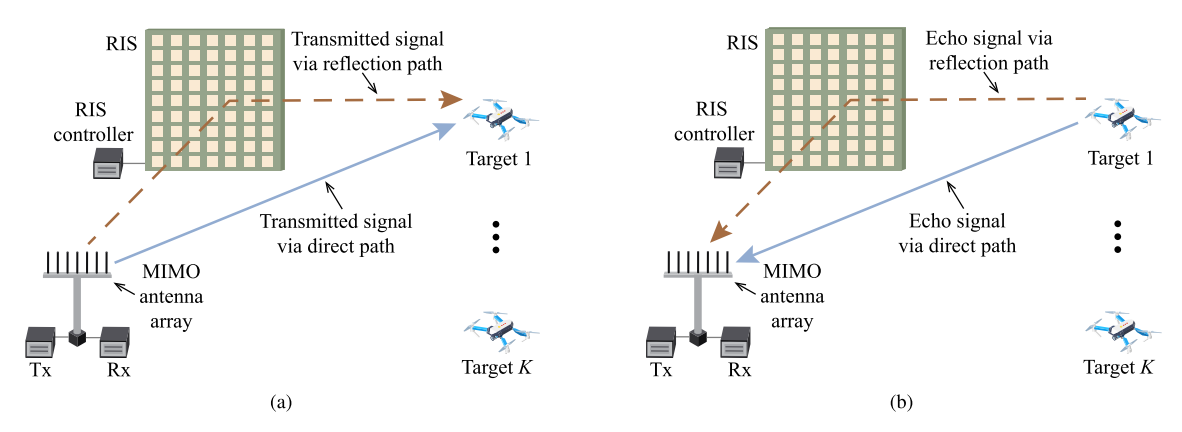


Fig. 14. MetaRadar system: (a) transmission mode and (b) reception mode.

In this section, the number of targets R is assumed to be unknown, but it falls within a known range. The space of interest (SOI) is discretized into multiple angular blocks, and each target is assumed to be located in one block. Given R and the direction of each target, the range of each target can be estimated based on the received signals. Therefore, a hypothesis U_i only needs to contain the number of targets and the directions of these targets, indicating the indices of the angular blocks. The multitarget detection is performed using multiple hypothesis testing techniques. Similar to the protocol introduced in Section III-A, the MetaRadar system is also operated in a synchronized manner, and the timeline is slotted into cycles. In each cycle, the following three steps are performed.

Optimization: The aim of the optimization step is to improve the detection performance by optimizing the radar waveforms and the RIS configuration. The detection performance can be quantified by the "distance" between the probability distributions of two different hypotheses. With the RIS, the received signal y is manipulated to maximize the distance between two hypotheses, and thus, any two hypotheses are more likely to be distinguished, leading to a higher detection accuracy. To be specific, the distance between hypotheses i and i' in the cth cycle can be defined as the relative entropy [45], i.e.,

$$d_{j,j'}^{c}(\mathcal{P}^{c}) = \text{KL}\left(p^{c}\left(\boldsymbol{y}\left|U_{j},\mathcal{P}^{c}\right.\right), p^{c}\left(\boldsymbol{y}\left|U_{j'},\mathcal{P}^{c}\right.\right)\right) + \text{KL}\left(p^{c}\left(\boldsymbol{y}\left|U_{j},\mathcal{P}^{c}\right.\right), p^{c}\left(\boldsymbol{y}\left|U_{j'},\mathcal{P}^{c}\right.\right)\right), \quad (18)$$

where $KL(\cdot)$ is the Kullback–Leibler divergence, \mathcal{P}^c is the set of optimization variables in the cth cycle, i.e., radar waveforms and RIS configuration, and $P^c(\boldsymbol{y}^c|U_j,\mathcal{P}^c)$ is the likelihood of receiving signal y^c given hypothesis U_i in the cth cycle, which can be expressed as

$$p^{c}(U_{j}, \mathcal{P}^{c}) = A \prod_{i=1}^{c} \exp\left(\frac{\left\|\boldsymbol{y}^{i} - \bar{\boldsymbol{y}}^{i} \left(U_{j}, \left\{\hat{\tau}_{r}^{j}\right\}_{r=1}^{R}, \hat{\boldsymbol{\gamma}}^{j}, \mathcal{P}^{c}\right)\right\|^{2}}{\sigma^{2}}\right).$$

$$(19)$$

Here, A is a scaling factor, σ^2 is the noise power, and $\bar{y}^i(U_j, \{\hat{\tau}_r^j\}_{r=1}^R, \hat{\gamma}^j, \mathcal{P}^c)$ denotes the expectation of signals received by the antenna array under hypothesis U_i in the ith cycle, delays from each target $\hat{\tau}_r^j$, and their responses $\hat{\gamma}^j$, where $\hat{\tau}_r^j$ and $\hat{\gamma}^j$ can be estimated jointly using the maximum likelihood estimation method.

To solve this problem efficiently, we first decouple the problem into two subproblems: the radar waveform optimization subproblem and the RIS configuration optimization subproblem. For the radar waveform optimization subproblem, this problem can be transformed into a quadratically constrained quadratic program (OCOP), which can be solved by the semidefinite relaxation (SDR) technique. For the RIS configuration optimization subproblem, the problem can also be transformed into a QCQP after relaxing the discrete phase shifts into continuous ones. After solving the QCQP, all the phase shifts will be recovered to the nearest available phase shift. More details can be found in [44].

Transmission and Reception: The optimized radar waveforms are transmitted. The RIS phase shifts are set as optimized in the previous step and could be different for transmission and reception modes. Then, the antenna array listens for the echo signals from the targets. Since the distances between the targets and the radar can be different, the echo signals from different targets may have different delays. The Rx will record these signals, including the delay information, for further processing.

Detection: In this step, the probability of each hypothesis will be updated. The prior probability distribution of these hypotheses is initialized to be uniform, where $p^1(U_i)$ is the initial probability for hypothesis U_j . Based on Bayes' formula, the probability update in the next cycle can be written as

$$p^{c+1}(U_j) = \frac{p^1(U_j)P^c(\mathbf{y}^c|U_j)}{\sum_{j'} p^1(U_{j'})P^c(\mathbf{y}^c|U_{j'})},$$
 (20)

where $P^c(\mathbf{y}^c|U_i)$ is the probability given in (19). At the end of the iteration, the hypothesis with the highest probability will be selected as the final result.

Zhang et al.: Toward Ubiquitous Sensing and Localization With Reconfigurable Intelligent Surfaces

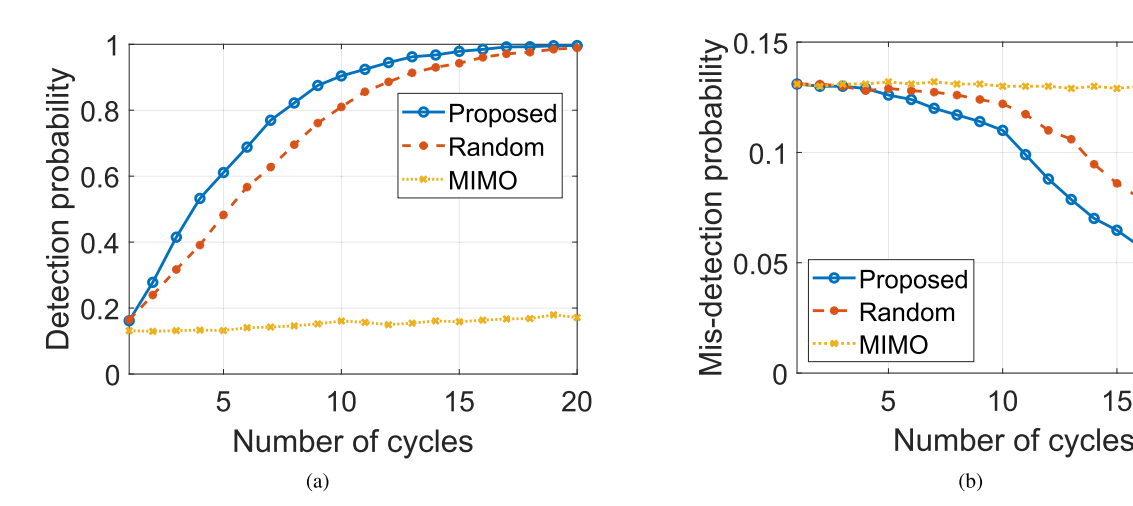


Fig. 15. Simulation results: (a) detection probability versus the number of cycles and (b) misdetection probability versus the number of cycles.

In Fig. 15, we show the detection probability and the misdetection probability versus the number of cycles for a typical example (details can be found in [44]). In comparison, we also present the results obtained by the standard MIMO radar and the RIS radar with a random RIS configuration. It can be observed that the detection probability obtained by the proposed scheme is higher, while the misdetection probability is smaller than those obtained by the other two schemes, which verifies the effectiveness of the proposed scheme. Moreover, we can also observe that the random and proposed schemes outperform the MIMO scheme. In particular, the growth rate of the detection probability obtained by the MIMO scheme is much lower than that of the others, and the detection probability obtained with the RIS can approach 1 after a sufficient number of cycles. Similarly, the misdetection probabilities obtained by the random and proposed schemes drop significantly faster than that obtained by the MIMO one. This has verified that incorporating the RIS can improve the performance of radar systems, even if the phase shifts of the RIS are not optimized by providing extra paths.

IV. RIS-AIDED LOCALIZATION

In this section, we will introduce RIS-aided RF localization applications. Similar to the sensing applications, the main challenge is to optimize the configurations of the RIS, especially when the size of the RIS is large. Based on the availability of prior information about the environment, the techniques can be broadly categorized into two types: MetaLocalization and MetaSLAM, which will be elaborated in Sections IV-A and IV-B, respectively.

A. MetaLocalization: Indoor Localization and Tracking

In this section, we will introduce how to localize/track users if prior knowledge of the environment can be known. For simplicity, we use RSS as the measurement metric.

In general, an RSS-based fingerprinting system consists of two phases: offline and online phases. In the offline phase, the system will collect the RSS value for each sampling location and generate a radio map. Then, in the online phase, the system will estimate the user's localization by comparing its measured RSS value with the radio map [46]. In an uncontrollable radio environment, as the radio map is passively measured, the RSS values for two neighboring locations might be similar to each other, leading to performance degradation. To address this issue, an RIS is used in an RF localization system to actively alter the radio maps and reduce the similarity of the RSS values corresponding to two adjacent locations. This type of system is referred to as MetaLocalization [47].

10

15

20

The MetaLocalization system is shown in Fig. 16. The system is composed of an AP, an RIS, and multiple users requiring indoor location services. The AP connects to the RIS controller to facilitate the synchronization. During the localization process, the AP sends a single-tone signal, and the RIS reflects the signal to users. Then, each user measures the RSS for localization. All the mobile users are assumed to move slowly or stay static in the SOI, which

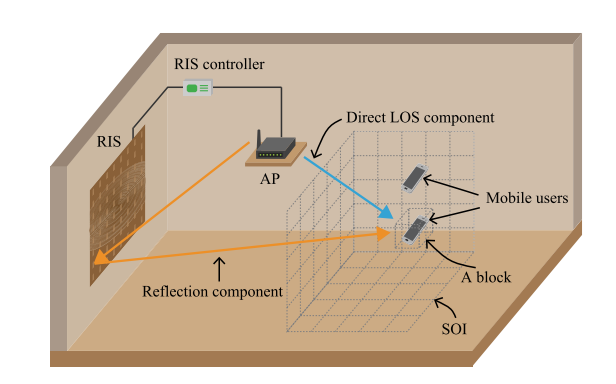


Fig. 16. Illustration for MetaLocalization systems.

is divided into several cubic blocks of the same size. The location of each user can be represented by the index of the block. The localization process has several cycles, each consisting of two phases: the radio map generation phase and the localization estimation phase, as introduced next.

1) Radio Map Generation Phase: To improve the localization accuracy, the MetaLocalization system needs to adjust the configurations of the RIS to reconfigure the radio environment and provide a favorable radio map. To be specific, for a certain configuration, the RSS for each block in the SOI can be calculated according to (12), and we can obtain the radio map by repeating this step for all the configurations. However, as the number of available configurations could be very large due to the size of the RIS, it is costly to measure the RSS values in the SOI for all the configurations.

To address this issue, we need to select a configuration that leads to the minimum localization loss in each cycle. More specifically, the localization loss can be defined as the sum of expected localization errors for all the users [48], which can be expressed as

$$l(\boldsymbol{c}, \mathcal{L}) = \sum_{i \in \mathcal{S}} \sum_{\substack{q, q' \in \mathcal{Q} \\ q \neq q'}} p_{i,q} \gamma_{q,q'} \int p(s_i | \boldsymbol{c}, q) \mathcal{L}(q' | \boldsymbol{c}, s_i) ds_i \quad (21)$$

where S is the set of users, Q is the set of blocks in the SOI, and c is the configuration of the RIS. Here, $p_{i,q}$ is the prior distribution of the users over the SOI, which can be obtained from the previous iteration. $\gamma_{q,q'}$ is the weight for the mislocalization, which is defined as the Euclidean distance between the ground-truth block q and the estimated block q'. This will force the estimated location to get closer to the ground-truth one as much as possible. $p(s_i|c,q)$ denotes the probability of the received RSS for user i being s_i with configuration cwhen user i is located at the qth block, and $\mathcal{L}(q'|c, s_i)$ is an estimation function to indicate whether user i is located at the q'th block with the received RSS s_i , which is assumed to be known in this phase and will be discussed in the following phase. Therefore, the integration is the probability that the system estimates user i to be located at the q'th block, while it is actually located at the qth block.

The loss function is nonconvex with respect to the RIS configuration c. Moreover, the configuration of the RIS is typically discrete in practice. To address this problem efficiently, we can first find some initial solutions and then use the global descent methods to update the solution, leading to a lower localization cost. The details of the algorithm can be found in [47].

2) Location Estimation Phase: Given configuration c and the RSS for each user s_i , the optimal estimation function, which yields to the minimum localization loss, can be

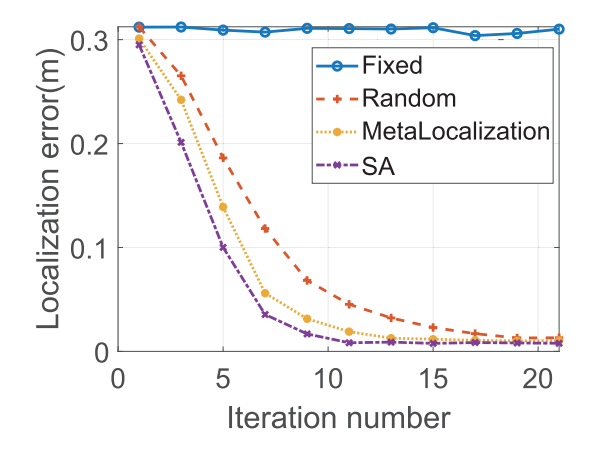


Fig. 17. Localization performance for a single user.

expressed as [47]

$$\mathcal{L}^*(q'|\mathbf{c}, s_i) = \begin{cases} 1, & s_i \in \mathcal{R}_{i,q'} \\ 0, & s_i \notin \mathcal{R}_{i,q'} \end{cases}$$
(22)

where the decision region $\mathcal{R}_{i,q'}$ is defined as

$$\mathcal{R}_{i,q'} = \left\{ s_i : \sum_{q \in \mathcal{Q}} p_{i,q} (\gamma_{q,q'} - \gamma_{q,q''}) p(s_i | \boldsymbol{c}, q) \le 0 \right.$$
$$\forall q'' \in \mathcal{Q} / \{q'\} \right\}. \tag{23}$$

The received RSS falling within the decision region implies that the localization loss will be less if we estimate that user i is located at the n'th block instead of the n''th block. Therefore, in this phase, each user can estimate its location using (22) according to the configuration c and the received RSS.

Fig. 17 shows the localization performance for a single user in a typical example (details can be found in [47]). To evaluate the performance of the MetaLocalization scheme, we also give the performance obtained by other three schemes: the fixed configuration scheme, the random configuration scheme, and the simulated annealing (SA) scheme. In the fixed configuration scheme, the states of all the RIS elements are fixed. In the random configuration scheme, random configurations are generated in different iterations. In the SA scheme, the SA method is utilized to optimize the RIS configurations, which can be regarded as a lower bound. We can observe that the localization error obtained by the fixed algorithm fluctuates between 0.30 and 0.32 m, while those obtained by the other three schemes decrease when the number of iterations increases. Moreover, we can observe that the localization error of the MetaLocalization scheme is close to that obtained

¹It is worth pointing out that the fixed configuration scheme can represent the case without the RIS. When the phase shifts of the RIS are fixed, the RIS can act as a normal wall that scatters the signals.

Zhang et al.: Toward Ubiquitous Sensing and Localization With Reconfigurable Intelligent Surfaces

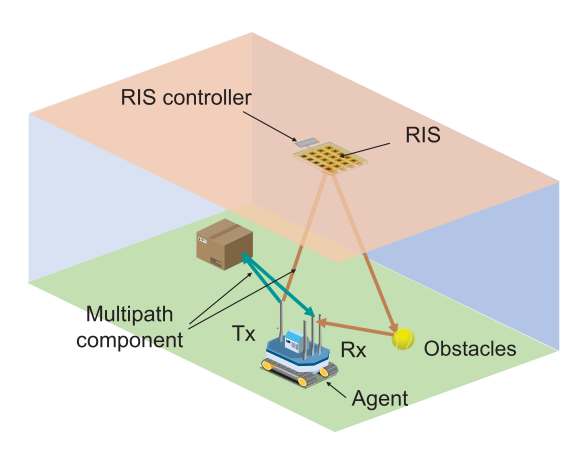


Fig. 18. Illustration for an indoor RIS-assisted SLAM scenario.

by the SA scheme, which can achieve centimeter-level localization accuracy. This indicates that the capability of the RIS to customize the propagation environment can improve the localization performance.

B. MetaSLAM: Simultaneous Localization and Mapping

In Section IV-A, we have introduced how to determine the users' locations if we have prior information about the environment. However, in some applications this may not be true; for example, a mobile robot is placed in an unknown environment to execute a certain task. How can this robot incrementally build a consistent map of this environment and locate itself within this map? To address this issue, the simultaneous localization and mapping (SLAM) technique was developed [49]. In the radiobased SLAM technique, the multipath propagation caused by scattering in the environment is exploited, and thus, the locations of objects in the environment (scatter points) are simultaneously determined with an agent of interest's location [50]. Even if the multipath channel is used as a constructive source of information in the localization problem, the related EM interactions with the environment still remain uncontrolled and, as such, largely suboptimal from the localization perspective [51]. This motivates us to leverage the RIS to improve the accuracy of the SLAM technique.

1) Indoor SLAM Scenario: A general indoor RIS-assisted SLAM scenario is shown in Fig. 18. An RIS is installed on the ceiling of a room and is linked to a controller that can change the phase shifts applied by the RIS to customize the propagation environment. A mobile agent is equipped with a single-antenna Tx and a multiple-antenna Rx. While moving in the room, the agent transmits signals and analyzes the received signals in order to locate itself and map the surrounding environment simultaneously. In particular, the agent first communicates with the RIS controller to adjust the phase shifts of the RIS. Next, the agent simultaneously emits signals to the environment and records the received signals, which contain multipath components

produced by the scattering and reflection of environmental obstacles and the RIS. The location of the mobile agent and environmental information can be extracted from these multipath components [53].

2) Multipath Component Modeling: Assume that the transmitted OFDM symbol $x^n(t)$ over the nth subcarrier travels via L paths to the vth Rx antenna. Therefore, the baseband OFDM symbol after removing the CP received by the vth Rx antenna at time t can be written as

$$y_v^n(t) = \sum_{l=1}^L \int_{-\infty}^{\infty} \hat{h}_{l,v}^n(\tau) x(t-\tau) d\tau + \omega_v^n(t)$$
 (24)

where $\hat{h}_{l,v}^n(t)$ denotes the CIR of the lth multipath channel to the vth Rx antenna over the nth subcarrier and $\omega_v^n(t)$ denotes Gaussian white noise.

In the following, we model the impulse response of channels via the obstacles and the RIS. Reflectors and scatterers are two types of obstacles that are considered. The reflectors are smooth surfaces like walls that receive a section of the incident wavefront and redirect it following the reflection law, while the scatterers only receive a point on the incident wavefront and diffusely scatter it in all directions. An example for the multipath channel is shown in Fig. 19.

a) Path through a reflector: As shown in Fig. 19, path 1 is the signal path from the Tx to the Rx via a reflector on the ceiling. The CIR of path 1 in general can be expressed as

$$\hat{h}_{1,v}^{n}(t) = h_{1,v}^{n} \delta(t - d_1/c) \tag{25}$$

where $h_{1,v}^n$ is the channel gain as introduced in (10), d_1 is the propagation length of this path, and $\delta(\cdot)$ is the delta function. As shown in Fig. 19, this CIR for this path is equivalent to that from a virtual Tx (VT), which is the

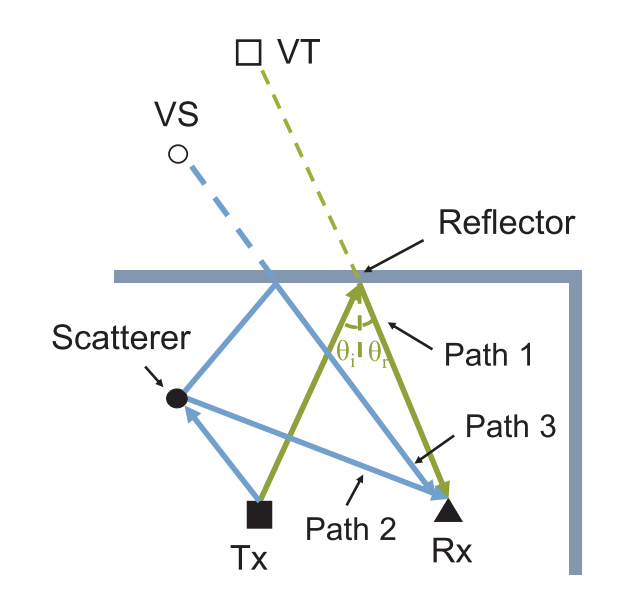


Fig. 19. Example for the multipath channel.

mirror image of the Tx. This presentation will be used in the following algorithm design.

- b) Path through a scatterer: As shown in Fig. 19, path 2 is the signal path from the Tx to the Rx via a scatterer. Its CIR can be expressed as that in (25), where the channel gain will be changed as defined in (11). It is worthwhile to point out that each RIS element can also be regarded as a scatterer with a controllable delay. If the scatterer is not an RIS element, γ_m should be set as 1 when calculating the channel gain according to (11).
- c) Path through a scatterer and a reflector: Path 3 is the propagation path from the Tx to the Rx via a scatterer and a reflector. Similarly, path 3 can be treated as being transmitted by a virtual scatterer (VS) with an additional delay introduced by the transmission between the Tx and the scatterer. The VS is also the mirror image of the scatterer, which will be used in the following algorithm design as well.
- 3) Position and Mapping Procedure: In the positioning and mapping procedure, we similarly divide the timeline into cycles. In each cycle, the following three steps are conducted sequentially.
- a) Step 1 (phase shift optimization): In this step, the agent needs to select the phase shifts of the RIS for the current cycle. The objective of this optimization problem is to minimize the localization error in the current cycle, i.e., the distance between the ground-truth and estimated locations. However, since the ground-truth location of the agent is unknown, it is difficult to optimize the phase shifts of the RIS with the positioning error as the objective. Alternatively, we use the Cramér–Rao lower bound (CRLB) to approximate the positioning error, which is widely used in the performance measurement of a SLAM system. In particular, the CRLB is reciprocal to the Fisher information matrix of the estimated location [52]. As the CRLB is nonconvex with respect to the phase shifts of the RIS, a genetic algorithm can be used to solve this problem [53].
- b) Step 2 (communication and measurement): After Step 1, the agent transmits a signal over a control channel carrying the phase shifts of the RIS to the RIS controller. The RIS controller will adjust the phase shifts accordingly. Once the phase shifts of the RIS are updated, the agent will transmit another signal for SLAM, and the Rx records the received signals at the same time.
- c) Step 3 (localization and mapping): The location of the agent and the map are updated based on the signals measured in Step 2. The localization and mapping procedure consists of two phases, i.e., the path grouping phase and the positioning and mapping phase.
 - 1) Path grouping phase: In this phase, we first need to recognize whether the received path is from a scatterer or a VS since scatterers and VSs are static. The Tx or VTs are moving during the SLAM process and thus cannot be used to locate the agent. The recognition can be achieved by a neural network [54]. Next, these paths are divided into several groups

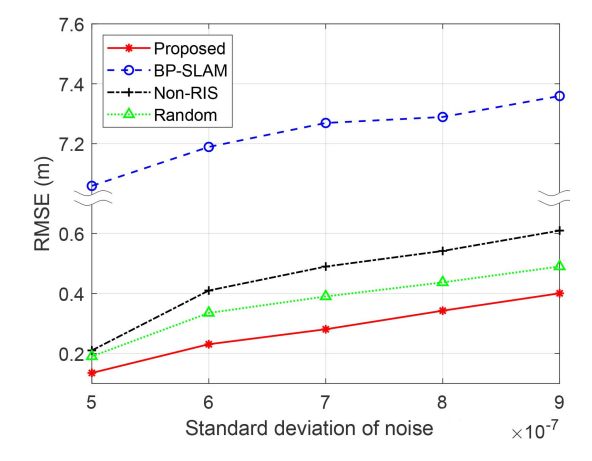


Fig. 20. Agent position RMSE versus standard deviation of noise.

based on their AoAs, each corresponding to a scatterer (including the RIS), which is also referred to as a landmark. The VS can be mapped with a scatterer according to the geometry. Finally, we need to decide which landmark is the RIS, which is necessary for the phase shift optimization. Let $p_{i,RIS}^c$ be the probability that the ith landmark is the RIS in the cth cycle, and we consider the probability obtained in the previous cycle to be the prior distribution for the current cycle. Based on Bayes' formula, we have

$$p_{i,\text{RIS}}^{c} = \frac{p_{i,\text{RIS}}^{c-1} p(\boldsymbol{a}^{c}|i\text{th landmark is the RIS})}{\sum_{i=1}^{N} p_{i,\text{RIS}}^{c-1} p(\boldsymbol{a}^{c}|i\text{th landmark is the RIS})}$$
(26)

where a^c denotes the amplitudes of paths extracted from the received signal y^c $p(a^c|ith \text{ landmark is the RIS})$ denotes the probability of receiving a^c if the ith landmark is the RIS. The landmark with the largest $p_{i,RIS}^c$ will be regarded as the RIS in the cth cycle.

2) Positioning and Mapping Phase: The positioning and mapping algorithm is based on the particle filter method [49]. The basic idea is to use a set of weighted particles to represent the probability distribution of the locations of the agent and landmarks, and the weights of these particles are updated based on the received signals. Since the estimation errors of ToFs and AoAs vary among different paths, we will optimize the weights of these paths in the particle filter to reduce the positioning errors. It is worth pointing out that the computational complexity increases exponentially with the number of landmarks held in the map. We can use partitioned updates and relative submaps to address this issue [55].

Fig. 20 shows the root-mean-square error (RMSE) of the estimated agent position versus the standard deviation of noise in a typical example (details can be found in [53]). In comparison, simulation results for the following three schemes are also provided.

Zhang et al.: Toward Ubiquitous Sensing and Localization With Reconfigurable Intelligent Surfaces

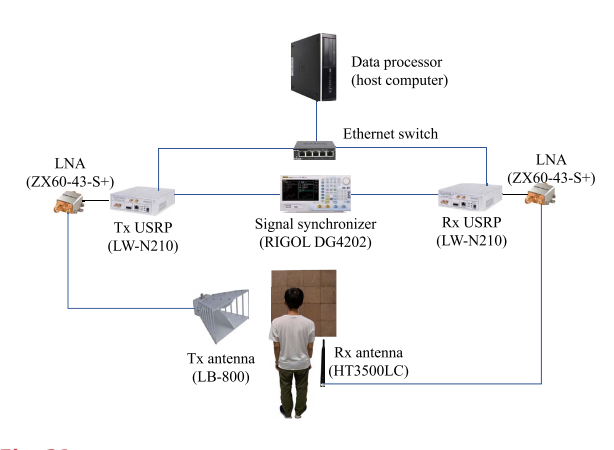


Fig. 21. Example prototype for RIS-aided wireless sensing and localization systems.

- 1) *Random scheme*: The phase shifts for the RIS are set randomly in each cycle.
- Non-RIS SLAM: There is no RIS in the room, and the agent performs SLAM using the proposed localization and mapping algorithm.
- BP-SLAM: This algorithm is proposed in [56], which only utilizes the TX and VTs for localization and mapping.

From this figure, we can observe that the RMSE of the agent's position obtained by the proposed scheme is at least 31% lower than those obtained by other benchmark schemes, which shows the superiority of the proposed SLAM scheme. Moreover, compared to those without the RIS, the RMSEs obtained by the RIS-aided SLAM systems are lower, implying the effectiveness of the RIS in improving the performance of SLAM systems.

V. SYSTEM IMPLEMENTATION AND EXPERIMENTAL EVALUATION

In Section V-A, we will introduce how to build an RIS-aided wireless sensing and localization hardware system, and in Section V-B, we will show some results obtained in the hardware systems.

A. System Components

An example prototype of an RIS-aided wireless sensing and localization system is shown in Fig. 21. In general, the system consists of two parts: the RIS and transceiver modules, which are elaborated as follows.

1) RIS Implementation: We use the electrically modulated RIS proposed in [57], which is shown in Fig. 22. The RIS is a 2-D array with a size of $69 \times 69 \times 0.52$ cm³, where each row/column of the array contains 48 RIS elements. Each RIS element has a size of $1.5 \times 1.5 \times 0.52$ cm³ and is composed of four rectangular copper patches printed on a dielectric substrate (Rogers 3010) with a dielectric constant of 10.2. Two adjacent copper patches are connected by a p-i-n diode (BAR 65-02L), and each p-i-n diode

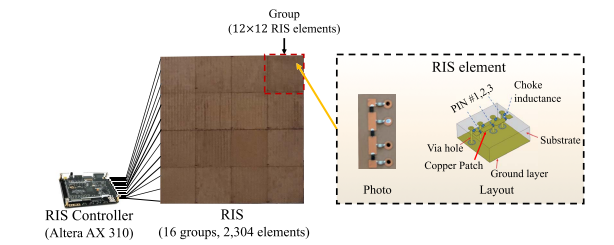


Fig. 22. RIS controller and RIS.

has two states, i.e., ON and OFF, which are controlled by applied bias voltages on the via holes. Besides, to isolate the DC feeding port and microwave signal, four choke inductors of 30 nH are used in each RIS element.

As shown in Fig. 22, three p-i-n diodes are included in an RIS element, and thus, an RIS element could have at most eight states. However, four states are used for the ease of control. Table 1 provides the amplitude and phase responses of an RIS element for these four states with the incident signals of 3.198 GHz [40]. Table 1 is obtained with the Microwave Studio and the Transient Simulation Package in the CST Studio Suite software package, by assuming normal illumination. In practice, to relieve the complexity of the control circuit, the RIS elements are divided into several groups, for example, 16 groups in this prototype, each containing 12×12 RIS elements arranged squarely. The RIS elements within the same group are in the same state.

As shown in Fig. 22, the states of these RIS elements are configured by an RIS controller, which is implemented by a field-programmable gate array (FPGA) (ALTERA AX301). In particular, the expansion ports on the FPGA are used for the configuration of the RIS. Every three expansion ports control the state of one group by applying bias voltages to the p-i-n diodes. The algorithms introduced in Sections III and IV are loaded onto the FPGA to automatically adjust the configurations of the RIS.

- 2) Transceiver Modules: As shown in Fig. 21, the transceiver module consists of the following components.
- 1) *Tx*: The Tx is implemented by using a universal software radio peripheral (USRP) device (LW N210). The USRP realizes the functions of RF modulation/demodulation and baseband signal processing by using the GNU Radio software development kit. The output port of the USRP is connected to a ZX60-43-S+ low-noise amplifier (LNA), which amplifies the transmitted signal. A directional double-ridged

Table 1 Amplitude and Phase Responses of an RIS Element

State	PIN # 1	PIN #2	PIN #3	Phase	Amplitude
1	OFF	OFF	OFF	$\pi/4$	0.97
2	ON	OFF	ON	$3\pi/4$	0.97
3	ON	OFF	ON	$5\pi/4$	0.92
4	ON	ON	OFF	$7\pi/4$	0.88

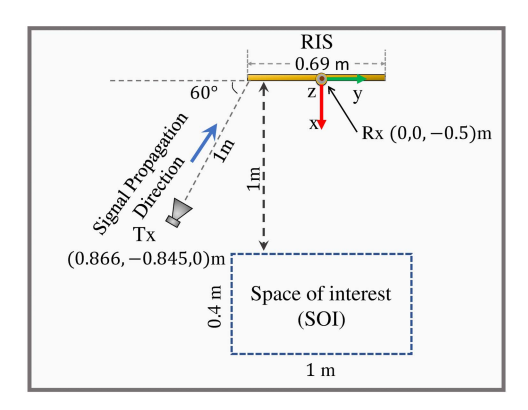


Fig. 23. Experimental layout for the MetaSensing system.

horn antenna (LB-880) is employed, which is linearly

- 2) Rx: Similar to the Tx, the Rx is a USRP, whose input port is connected to an LNA, and an omnidirectional vertical antenna (HT3500LC) is utilized. An external clock (10-MHz OCXO) is used to provide a precise clock signal to the Tx and Rx.
- 3) Signal synchronizer: To obtain the relative phases and amplitudes of the received signals with respect to the transmitted signals, we employ a signal source (RIGOL DG4202) to synchronize the Tx and Rx USRPs. The signal source provides the reference clock signal and the pulse-per-second (PPS) signal to the USRPs, which are used for the modulation and demodulation. For the phase synchronization, the Tx and Rx USRPs are connected by a wired link with a fixed gain, which is used to compensate for the instrumental error of the USRPs.
- 4) Ethernet switch: This connects the USRPs and a host computer to a common Ethernet where they exchange the transmitted and received signals.
- 5) Data processor: This is a host computer that controls the Tx and Rx using Python programs. The host computer also extracts and processes the received signals.

B. Performance Evaluation

In this section, we will show some experimental results obtained from the shown prototype to validate the effectiveness of the proposed RIS-assisted wireless sensing and localization schemes.

1) RIS-Aided Sensing: For sensing applications, we use posture recognition as an example. In this experiment, we consider four postures for recognition: standing, sitting, bending, and lying down. For each posture, we collect 150 labeled measurements with a random configuration and an optimized configuration of the RIS and form the datasets.

The layout of the experiment is shown in Fig. 23. The origin of the 3-D coordinate system is located at the center of the RIS, and the RIS is in the yz plane. The z-axis is vertical to the ground and pointing upward, and the x- and y-axes are parallel to the ground. The Tx antenna is located 1 m away from the corner of the RIS and the Rx antenna is placed below the RIS. The human body is in the SOI, which is a cuboid region located 1 m from the RIS. The side lengths of the SOI are $l_x = 0.4$ m, $l_y = 1.0$ m, and $l_z = 1.6$ m. Moreover, the SOI is further divided into M=80 cubes with a side length of 0.2 m. For more detailed experimental settings, please refer to [40].

Fig. 24 shows the accuracy of the posture recognition with the optimized configuration, random configuration, and no-RIS. In each subfigure, the diagonal elements are the recognition accuracy for each posture. It can be observed that the system with optimized configuration can achieve 14.6% higher recognition accuracy compared to that with random configuration. This verifies the necessity of the phase shift optimization. Moreover, compared to the no-RIS case, we can observe that the RIS can significantly increase the posture recognition accuracy even with a random recognition. This justifies the effectiveness of RIS-aided RF sensing.

2) RIS-Aided Localization: For localization applications, we show the MetaLocalization system as an example. We perform the experiments in a classroom with a size of 25 m², and the walls of the classroom are made of bricks and concrete. As shown in Fig. 25, the SOI is a cubic region with dimensions $0.5 \times 0.5 \times 0.5 \text{ m}^3$. The center of the SOI is 1 m away from the center of the RIS. When building the radio map for each SOI, we discretize the SOI into blocks and record the signals for each block. No objects exist between the users and the RIS. Please refer to [59] for further experimental details.

Fig. 26 shows the process of multiuser localization without obstruction. For display simplicity, in this figure, we choose a planar SOI that is on the plane z = 0 with dimensions $0.5 \times 0.5 \text{ m}^2$ and the distance to the RIS is 1 m. The users' ground-truth locations are labeled in the figures by the red triangle (the first user), yellow circle (the second user), and the black star (the third user). We can observe that the RSS varies for different iterations. The probabilities are approximately uniformly distributed in each location in the first cycle (first row of subfigures), while after several cycles, the probabilities of locations near the ground truth are obviously higher than those in the other locations, which confirms the effectiveness of the MetaLocalization scheme. We can also observe that the locations in the x-direction near the ground truth have higher probabilities than the locations in the y-direction, indicating that it is more likely to misjudge the x-coordinate than the y-coordinate of the user's location. Because the x-axis is perpendicular to the RIS, the correlation of signals on the x-axis is higher than those on the y- and z-axes, thus leading to higher localization error.

VI. FUTURE DIRECTIONS

In the previous sections, we have presented some case studies to illustrate how to integrate RISs with wireless

Zhang et al.: Toward Ubiquitous Sensing and Localization With Reconfigurable Intelligent Surfaces

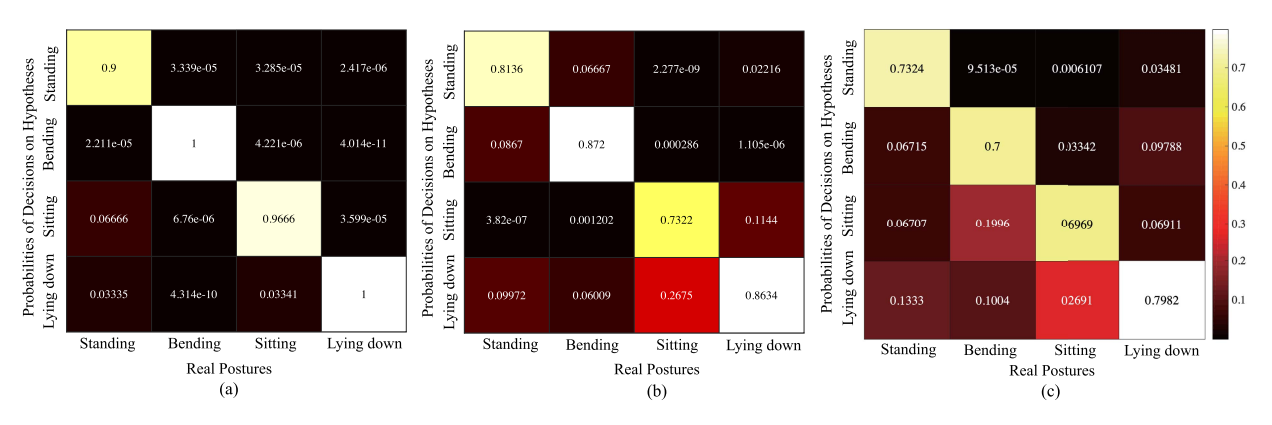


Fig. 24. Posture recognition accuracy with (a) optimized configuration, (b) random configuration, and (c) No-RIS.

networks to achieve ubiquitous sensing and localization, and we have introduced how to build prototypes. In the following, we will further discuss some other relevant topics that are worthy of further investigation.

A. Mobility

In the previous case studies, we have focused on static or slow-moving targets, where the targets/users stay in the same block within a cycle. However, in practical scenarios, the targets/users might move at relatively high speeds, e.g., vehicles, which implies that they will be in different blocks within a cycle. Therefore, it is also necessary to develop new techniques for such use cases by exploiting the relations among these blocks.

Different from the traditional methods for moving targets/users [60], where the motion is captured by the signal processing techniques at the Rx, the RIS-aided localization and sensing systems can leverage the capability to configure the RIS based on the motion of the targets to achieve higher sensing or localization accuracy. However, if we only configure the RIS based on predicted locations, estimation errors in previous slots might accumulate, leading to a low RSS from the objects. As a result, how to develop an effective RIS configuration scheme according to the movement of objects still remains an open problem. On the other hand, the signal processing techniques at the Rx will also be different. The

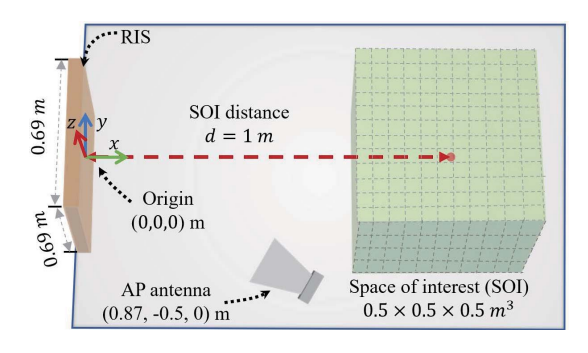


Fig. 25. Experimental layout for the MetaLocalization system.

RIS configuration also influences the RSS and should be jointly designed with the estimation procedure. Therefore, how to estimate the locations of moving targets is a challenge.

B. Millimeter-Wave and Terahertz Bands

The higher frequency bands, including millimeter-wave (mmWave) and THz bands, are promising candidates for sensing and localization applications as they can provide fine resolution in range and angle. However, the higher frequency bands suffer from high propagation losses and power limitations, which results in a short sensing and localization range [61]. Benefiting from the capability to customize the propagation environment, the RIS has shown its potential to improve the range, but the combination of RISs and mmWave and THz bands also brings some unique challenges for RF sensing and localization use cases.

- Hardware complexity: The RIS is typically designed to operate over a predefined frequency band, and the implementation complexity is positively proportional to the working frequency, as the size of the RIS element should be on the order of the wavelength. Moreover, using higher frequencies also requires faster response time for changing phase shifts.
- 2) Signal processing: Higher frequency bands have some unique characteristics that require the development of some signal processing techniques specific to these bands. For example, the path loss of a THz signal in the presence of water vapor is dominated by spikes that represent molecular absorption losses due to molecular vibrations [62]. As a result, the spectrum is divided into small subbands, and these subbands are distance-dependent. Therefore, it is important to consider these physical features when designing the decision function for sensing and localization purposes.

C. Security and Privacy

The rapid development of wireless and localization technologies has led to the flourishing of location-based

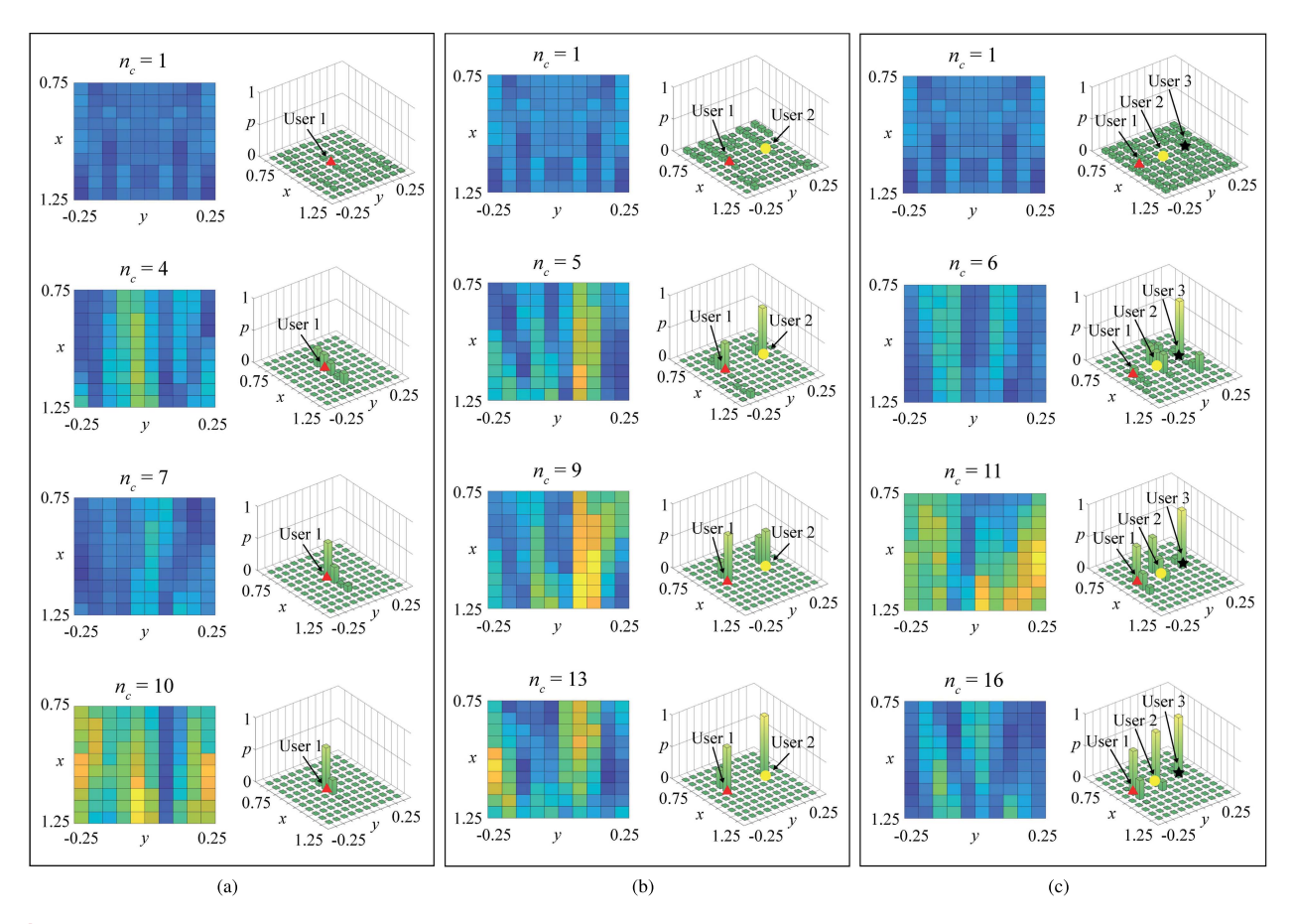


Fig. 26. Illustrations of the MetaLocalization scheme without obstruction for three users: (a) one user, (b) two users, and (c) three users. The first column in each subfigure shows the radio maps after different cycles, and the second column shows the corresponding probability distribution for different locations. Here, the probability is the sum of the probabilities of all the users. These three users' ground-truth locations are denoted by the red triangle, the yellow circle, and the black star.

services (LBSs), where delivered information is customized according to users' physical locations. Although LBSs can provide enhanced functionalities, they also open up new vulnerabilities that can be used to cause security and privacy issues [63]. For example, location information privacy is becoming critical in various applications, such as health monitoring, social media, and surveillance systems, as we can infer some sensitive information from users' locations. Therefore, it is important to preserve users' privacy and security.

As listed in the following, the adoption of RISs in localization systems brings some unique challenges and research directions for the preservation of users' privacy and security.

1) Privacy preserving mechanisms: In location-based systems, there are some existing privacy-preserving mechanisms, such as mix zones, dummy-based mechanisms, and perturbation-based mechanisms [64]. However, these mechanisms cannot be applied in RIS-aided localization systems since we might also infer users' locations from the configurations of the RIS. Therefore, it is necessary to

- consider the tradeoff between accuracy and privacy when optimizing the configuration of the RIS.
- 2) Secure localization methods: Although the RIS provides the opportunity to customize the propagation environment, it will also become an attack target, leading to new security issues. For example, if the RIS is attacked and its configuration is not consistent with that computed at the BS, the estimated location will be quite different from the ground-truth one, which might cause severe consequences in many critical applications. Therefore, it is also important for the RIS-assisted localization systems to detect any misbehavior of the RIS.

D. Integrated Sensing and Communication Design

In general, sensing and communication systems are deployed separately and use different frequency bands. However, with the increasing number of connected devices and services in the wireless communication industry, the frequency is becoming congested. This motivates us to consider the integration of sensing and communication to further improve the spectral efficiency [65]. As a result, the integrated sensing and communication (ISAC) system

needs to be well designed to achieve a desirable performance tradeoff between sensing and communication.

In RIS-aided sensing systems, it is not easy to integrate both sensing and communication functions. Some possible challenges and research directions are listed as follows.

- 1) Channel modeling: The algorithms for sensing functions highly depend on the location of targets and the surrounding environment. This cannot be captured by the stochastic channel models that are widely used for wireless communications. To this end, ray tracing could be a strong candidate for channel modeling [66]. However, the existence of the RIS makes ray tracing more complicated as the RIS might introduce multihop scattering. Therefore, it is essential to develop a new channel modeling method to accommodate RIS-assisted ISAC systems.
- 2) Waveform design: In the ISAC system, a single RF signal should convey both communication and sensing data. Therefore, the waveform design is important but challenging due to the contradicting metrics for communication and sensing. In particular, the main target for communication systems is to maximize the spectral efficiency [67], while optimal waveforms for sensing are designed for higher sensing resolution and accuracy. Therefore, attention needs to be paid to waveform design to strike a balance between communication and sensing performance.
- 3) RIS configuration: The deployment of an RIS in an ISAC system can shape the radio environment by adjusting the phase responses of each RIS element

in order to improve both sensing and communication performance. This requires an appropriate design for the configuration of the RIS. However, the optimization of the RIS configuration is not trivial. First, in practical systems, the number of possible phase shifts applied to each RIS element is finite [68]. As a result, the feasibility set for the optimization problem is discrete, leading to an NP-hard integer program. Second, the RIS configuration is, in general, coupled with the waveform design, which makes it more complicated. Machine learning methods might be a useful tool to address this issue. Moreover, how to place the RIS to obtain a better performance is another interesting topic [69].

VII. CONCLUSION

In this article, we have provided a comprehensive tutorial on the application of the innovative RIS technique to wireless sensing and localization use cases. Benefiting from its capability to customize the wireless propagation environment, RISs have shown the potential to enhance the difference of the received signals from neighboring targets/locations, thus improving the accuracy of sensing and localization. This article has reviewed the preliminaries, state-of-the-art results on the main challenges for wireless sensing and localization applications, and future research directions. We hope that this article can be a useful resource for future research on RIS-aided wireless sensing and localization, unlocking its full potential in future wireless systems.

REFERENCES

- T. Wild, V. Braun, and H. Viswanathan, "Joint design of communication and sensing for beyond 5G and 6G systems," *IEEE Access*, vol. 9, pp. 30845–30857, 2021
- [2] A. Bourdoux et al., "6G white paper on localization and sensing," 2020, arXiv:2006.01779.
- [3] Study NR Positioning Support, document 3GPP TR 38.855, TR16, 2018.
- [4] X. You et al., "Towards 6G wireless communication networks: Vision, enabling technologies, and new paradigm shifts," Sci. China Inf. Sci., vol. 64, no. 1, Jan. 2021, Art. no. 110301.
- [5] H. Zhang, B. Di, L. Song, and Z. Han, Reconfigurable Intelligent Surface-Empowered 6G. Cham, Switzerland: Springer, 2021.
- [6] M. Di Renzo et al., "Smart radio environments empowered by reconfigurable intelligent surfaces: How it works, state of research, and the road ahead," *IEEE J. Sel. Areas Commun.*, vol. 38, no. 11, pp. 2450–2525, Nov. 2020.
- [7] Z. Yang et al., "Energy-efficient wireless communications with distributed reconfigurable intelligent surfaces," *IEEE Trans. Wireless Commun.*, vol. 21, no. 1, pp. 665–679, Jan. 2022.
- [8] M. A. El Mossallamy, H. Zhang, L. Song, K. G. Seddik, Z. Han, and G. Y. Li, "Reconfigurable intelligent surfaces for wireless communications: Principles, challenges, and opportunities," *IEEE Trans. Cogn. Commun. Netw.*, vol. 6, no. 3, pp. 990–1002, Sep. 2020.
- [9] F. Tariq, M. R. A. Khandaker, K.-K. Wong, M. A. Imran, M. Bennis, and M. Debbah, "A speculative study on 6G," *IEEE Wireless Commun.*, vol. 27, no. 4, pp. 118–125, Aug. 2020.
- [10] K. Witrisal et al., "High-accuracy localization for assisted living: 5G systems will turn multipath channels from foe to friend," IEEE Signal Process.

- Mag., vol. 33, no. 2, pp. 59–70, Mar. 2016.
 [11] E. S. Lohan *et al.*, "Benefits of positioning-aided
- communication technology in high-frequency industrial lof," *IEEE Commun. Mag.*, vol. 56, no. 12, pp. 142–148, Dec. 2018.
 [12] B. Paden, M. Čáp, S. Z. Yong, D. Yershov, and
- E. Frazzoli, "A survey of motion planning and control techniques for self-driving urban vehicles," *IEEE Trans. Intell. Veh.*, vol. 1, no. 1, pp. 33–55, Mar. 2016.
- [13] P. Wang, B. Di, H. Zhang, K. Bian, and L. Song, "Cellular V2X communications in unlicensed spectrum: Harmonious coexistence with VANET in 5G systems," *IEEE Trans. Wireless Commun.*, vol. 17, no. 8, pp. 5212–5224, Aug. 2018.
- [14] H. Wang, D. Zhang, Y. Wang, J. Ma, Y. Wang, and S. Li, "RT-Fall: A real-time and contactless fall detection system with commodity WiFi devices," *IEEE Trans. Mobile Comput.*, vol. 16, no. 2, pp. 511–526, Feb. 2017.
- [15] S. A. Shah and F. Fioranelli, "RF sensing technologies for assisted daily living in healthcare: A comprehensive review," *IEEE Aerosp. Electron.* Syst. Mag., vol. 34, no. 11, pp. 26–44, Nov. 2019.
- [16] J. Wei, Q. Gao, M. Pan, and Y. Fang, "Device-free wireless sensing: Challenges, opportunities, and applications," *IEEE Netw.*, vol. 32, no. 2, pp. 132–137, Mar. 2018.
- [17] J. Liu, H. Liu, Y. Chen, Y. Wang, and C. Wang, "Wireless sensing for human activity: A survey," *IEEE Commun. Surveys Tuts.*, vol. 22, no. 3, pp. 1629–1645, 3rd Quart., 2020.
- [18] R. Zekavat and R. M. Buehrer, Handbook of Position Location: Theory, Practice and Advances. Hoboken, NJ, USA: Wiley, 2011.
- [19] S. Y. Seidel and T. S. Rappaport, "914 MHz path loss prediction models for indoor wireless

- communications in multifloored buildings," *IEEE Trans. Antennas Propag.*, vol. 40, no. 2, pp. 207–217, Feb. 1992.
- [20] Y. Wang, J. Liu, Y. Chen, M. Gruteser, J. Yang, and H. Liu, "E-eyes: Device-free location-oriented activity identification using fine-grained WiFi signatures," in Proc. ACM Annu. Int. Conf. Mobile Comput. Netw. (MobiCom), Maui, HI, USA, Sep. 2014, pp. 617–628.
- [21] I. Guvenc and C.-C. Chong, "A survey on TOA based wireless localization and NLOS mitigation techniques," *IEEE Commun. Surveys Tuts.*, vol. 11, no. 3, pp. 107–124, Aug. 2009.
- [22] Z. He, Y. Ma, and R. Tafazolli, "Improved high resolution TOA estimation for OFDM-WLAN based indoor ranging," *IEEE Wireless Commun. Lett.*, vol. 2, no. 2, pp. 163–166, Apr. 2013.
- [23] X. Li and K. Pahlavan, "Super-resolution TOA estimation with diversity for indoor geolocation," *IEEE Trans. Wireless Commun.*, vol. 3, no. 1, pp. 224–234, Jan. 2004.
- [24] B. H. Fleury, M. Tschudin, R. Heddergou, D. Dahlhaus, and K. I. Pedersen, "Channel parameter estimation in mobile radio environments using the SAGE algorithm," *IEEE J. Sel. Areas Commun.*, vol. 17, no. 3, pp. 434–449, Mar. 1999.
- [25] C. Iovescu and S. Rao, "The fundamentals of millimeter wave sensors," Texas Instrum., Dallas, TX, USA, Tech. Rep., 2017.
- [26] A. Goldsmith, Wireless Communications. Cambridge, U.K.: Cambridge Univ. Press, 2005.
- [27] M. Di Renzo et al., "Smart radio environments empowered by reconfigurable AI meta-surfaces: An idea whose time has come," EURASIP J. Wireless Commun. Netw., vol. 2019, no. 1, pp. 1–20, May 2019.
- [28] H.-T. Chen, W. J. Padilla, J. M. O. Zide,

- A. C. Gossard, A. J. Taylor, and R. D. Averitt, "Active terahertz metamaterial devices," Nature, vol. 444, pp. 597-600, Nov. 2006.
- [29] B. Di, H. Zhang, L. Li, L. Song, Y. Li, and Z. Han, "Practical hybrid beamforming with finite-resolution phase shifters for reconfigurable intelligent surface based multi-user communications," IEEE Trans. Veh. Technol., vol. 69, no. 4, pp. 4565-4570, Apr. 2020.
- [30] S. Zeng et al., "Reconfigurable intelligent surfaces in 6G: Reflective, transmissive, or both?" IEEE Commun. Lett., vol. 25, no. 6, pp. 2063-2067, Jun. 2021.
- [31] X. Yu, D. Xu, Y. Sun, D. W. K. Ng, and R. Schober, "Robust and secure wireless communications via intelligent reflecting surfaces," IEEE J. Sel. Areas Commun., vol. 38, no. 11, pp. 2637-2652, Nov. 2020.
- [32] H. Zhang et al., "Intelligent omni-surfaces for full-dimensional wireless communications: Principles, technology, and implementation," IEEE Commun. Mag., vol. 60, no. 2, pp. 39-45, Feb. 2022.
- [33] S. Zhang, H. Zhang, B. Di, Y. Tan, Z. Han, and L. Song, "Reflective-transmissive metasurface aided communications for full-dimensional coverage extension," IEEE Trans. Veh. Technol., vol. 69, no. 11, pp. 13905-13909, Nov 2020
- [34] B. Di, H. Zhang, L. Song, Y. Li, Z. Han, and H. V. Poor, "Hybrid beamforming for reconfigurable intelligent surface based multi-user communications: Achievable rates with limited discrete phase shifts," IEEE J. Sel. Areas Commun., vol. 38, no. 8, pp. 1809-1822, Aug. 2020.
- [35] Y. Liu et al., "Reconfigurable intelligent surfaces: Principles and opportunities," IEEE Commun. Surveys Tuts., vol. 23, no. 3, pp. 1546-1577, 3rd Quart., 2021.
- [36] S. Zhang et al., "Intelligent omni-surfaces: Ubiquitous wireless transmission by reflective-refractive metasurfaces,"IEEE Trans.Wireless Commun., vol. 21, no. 1, pp. 219-233,
- [37] H. Zhang, B. Di, Z. Han, H. V. Poor, and L. Song, "Reconfigurable intelligent surface assisted multi-user communications: How many reflective elements do we need?" IEEE Wireless Commun. Lett., vol. 10, no. 5, pp. 1098-1102, May 2021.
- [38] W. Tang et al., "Wireless communications with reconfigurable intelligent surface: Path loss modeling and experimental measurement," IEEE Trans. Wireless Commun., vol. 20, no. 1, pp. 421-439, Jan. 2021.
- [39] J. Hu, H. Zhang, K. Bian, M. D. Renzo, Z. Han, and L. Song, "MetaSensing: Intelligent metasurface assisted RF 3D sensing by deep reinforcement learning," IEEE J. Sel. Areas Commun., vol. 39, no. 7, pp. 2181-2197, Jul. 2021.
- [40] J. Hu et al., "Reconfigurable intelligent surfaces based radio-frequency sensing: Design, optimization, and implementation," IEEE J. Sel. Areas Commun., vol. 38, no. 11, pp. 2700-2716, Nov. 2020.

- [41] M. Elad, "Optimized projections for compressed sensing," IEEE Trans. Signal Process., vol. 55, no. 12, pp. 5695-5702, Dec. 2007.
- [42] I. Goodfellow, Y. Bengio, A. Courvile, and Y. Bengio, Deep Learning. Cambridge, MA, USA: MIT Press,
- [43] J. Hu, H. Zhang, K. Bian, Z. Han, H. V. Poor, and L. Song, "MetaSketch: Wireless semantic segmentation by reconfigurable intelligent surfaces," IEEE Trans. Wireless Commun., early access, Jan. 26, 2022, doi: 10.1109/TWC.2022.3144340.
- [44] H. Zhang, H. Zhang, B. Di, K. Bian, Z. Han, and L. Song, "MetaRadar: Multi-target detection for reconfigurable intelligent surface aided radar systems," IEEE Trans. Wireless Commun., early access, Mar. 2, 2022, doi: 10.1109/TWC.2022.3153792
- [45] L. Wang, W. Zhu, Y. Zhang, Q. Liao, and J. Tang, "Multi-target detection and adaptive waveform design for cognitive MIMO radar," IEEE Sensors J., vol. 18, no. 24, pp. 9962–9970, Dec. 2018.
- [46] Z. Yang, C. Wu, and Y. Liu, "Locating in fingerprint space: Wireless indoor localization with little human intervention," in Proc. 18th Annu. Int. Conf. Mobile Comput. Netw. (Mobicom), Istanbul, Turkey, Aug. 2012, pp. 269-280.
- [47] H. Zhang, H. Zhang, B. Di, K. Bian, Z. Han, and L. Song, "MetaLocalization: Reconfigurable intelligent surface aided multi-user wireless indoor localization," IEEE Trans. Wireless Commun. vol. 20, no. 12, pp. 7743-7757, Dec. 2021.
- [48] H. Zhang, H. Zhang, B. Di, K. Bian, Z. Han, and L. Song, "Towards ubiquitous positioning by leveraging reconfigurable intelligent surface," ${\it IEEE}$ Commun. Lett., vol. 25, no. 1, pp. 284-288, Jan. 2021.
- [49] H. Durrant-Whyte and T. Bailey, "Simultaneous localization and mapping: Part I," IEEE Robot. Autom. Mag., vol. 13, no. 2, pp. 99-110, Jun. 2006.
- [50] C. Gentner, T. Jost, W. Wang, S. Zhang, A. Dammann, and U.-C. Fiebig, "Multipath assisted positioning with simultaneous localization and mapping," IEEE Trans. Wireless Commun., vol. 15, no. 9, pp. 6104-6117, Sep. 2016.
- [51] H. Wymeersch, J. He, B. Denis, A. Clemente, and M. Juntti, "Radio localization and mapping with reconfigurable intelligent surfaces: Challenges, opportunities, and research directions," IEEE Veh. Technol. Mag., vol. 15, no. 4, pp. 52-61, Dec. 2020.
- K. Witrisal and P. Meissner, "Performance bounds for multipath-assisted indoor navigation and tracking (MINT)," in Proc. IEEE Int. Conf. Commun. (ICC), Ottawa, ON, Canada, Jun. 2012, pp. 4321-4325.
- [53] Z. Yang, H. Zhang, B. Di, H. Zhang, K. Bian, and L. Song, "Wireless indoor simultaneous localization and mapping using reconfigurable intelligent surface," in Proc. IEEE Global Commun. Conf. (GLOBECOM), Madrid, Spain, Dec. 2021, pp. 1-6.
- [54] S. Thrun, W. Burgard, and D. Fox, Probabilistic Robotics (Intelligent Robotics and Autonomous Agents). Cambridge, MA, USA: MIT Press,
- [55] T. Bailey and H. Durrant-Whyte, "Simultaneous

- localization and mapping (SLAM): Part II," IEEE Robot. Autom. Mag., vol. 13, no. 3, pp. 108-117, Sep. 2006.
- [56] E. Leitinger, F. Meyer, F. Hlawatsch, K. Witrisal, F. Tufvesson, and M. Z. Win, "A belief propagation algorithm for multipath-based SLAM," IEEE Trans. Wireless Commun., vol. 18, no. 12, pp. 5613-5629, Dec. 2019.
- [57] L. Li et al., "Machine-learning reprogrammable metasurface imager," Nature Commun., vol. 10, no. 1, p. 1082, Jun. 2019.
- [58] E. Blossom, "GNU radio: Tools for exploring the radio frequency spectrum," J. Linux, vol. 2004, no. 122, p. 4, Jun. 2004.
- [59] H. Zhang et al., "MetaRadar: Indoor localization by reconfigurable metamaterials," IEEE Trans. Mobile Comput., early access, Dec. 14, 2020, doi: 10.1109/TMC.2020.3044603
- [60] C. Wu, Z. Yang, Z. Zhou, X. Liu, Y. Liu, and J. Cao, "Non-invasive detection of moving and stationary human with WiFi," IEEE J. Sel. Areas Commun., vol. 33, no. 11, pp. 2329-2342, Nov. 2015.
- [61] H. Sarieddeen, N. Saeed, T. Y. Al-Naffouri, and M.-S. Alouini, "Next generation terahertz communications: A rendezvous of sensing, imaging, and localization," IEEE Commun. Mag., vol. 58, no. 5, pp. 69-75, May 2020.
- [62] H. Sarieddeen, M.-S. Alouini, and T. Y. Al-Naffouri, "An overview of signal processing techniques for terahertz communications," Proc. IEEE, vol. 109, no. 10, pp. 1628-1665, Oct. 2021.
- [63] M. Min et al., "3D geo-indistinguishability for indoor location-based services," IEEE Trans. Wireless Commun., early access, Dec. 10, 2021, doi: 10.1109/TWC.2021.3132464.
- [64] V. Primault, A. Boutet, S. B. Mokhtar, and L. Brunie, "The long road to computational location privacy: A survey," IEEE Commun. Surveys Tuts., vol. 21, no. 3, pp. 2772-2793, 3rd Quart., 2019.
- [65] F. Liu, C. Masouros, A. P. Petropulu, H. Griffiths, and L. Hanzo, "Joint radar and communication design: Applications, state-of-the-art, and the road ahead," IEEE Trans. Commun., vol. 68, no. 6, pp. 3834-3862, Jun. 2020.
- [66] D. K. P. Tan et al., "Integrated sensing and communication in 6G: Motivations, use cases, requirements, challenges and future directions," in Proc. 1st IEEE Int. Symp. Commun. Sens. (JC S), Dresden, Germany, Feb. 2021, pp. 1-6.
- X. Cao, B. Yang, H. Zhang, C. Huang, C. Yuen, and Z. Han, "Reconfigurable-intelligent-surface-assisted MAC for wireless networks: Protocol design, analysis, and optimization," IEEE Internet Things J., vol. 8, no. 18, pp. 14171–14186, Sep. 2021.
- [68] H. Zhang, B. Di, L. Song, and Z. Han, "Reconfigurable intelligent surfaces assisted communications with limited phase shifts: How many phase shifts are enough?" IEEE Trans. Veh. Technol., vol. 69, no. 4, pp. 4498-4502, Apr. 2020.
- [69] S. Zeng, H. Zhang, B. Di, Z. Han, and L. Song, "Reconfigurable intelligent surface (RIS) assisted wireless coverage extension: RIS orientation and location optimization," IEEE Commun. Lett., vol. 25, no. 1, pp. 269-273, Jan. 2021.

ABOUT THE AUTHORS

Hongliang Zhang (Member, IEEE) received the B.S. and Ph.D. degrees from the School of Electrical Engineering and Computer Science, Peking University, Beijing, China, in 2014 and 2019, respectively.

He was a Postdoctoral Fellow with the Department of Electrical and Computer Engineering, University of Houston, Houston, TX, USA. He is currently a Postdoc-

toral Associate with the Department of Electrical and Computer Engineering, Princeton University, Princeton, NJ, USA. His current research interest includes reconfigurable intelligent surfaces, aerial access networks, optimization theory, and game theory.



Dr. Zhang received the Best Doctoral Thesis Award from the Chinese Institute of Electronics in 2019. He is an Exemplary Reviewer for IEEE TRANSACTIONS ON COMMUNICATIONS in 2020. He was a recipient of the 2021 IEEE Comsoc Heinrich Hertz Award for Best Communications Letters and the 2021 IEEE ComSoc Asia-Pacific Outstanding Paper Award. He has served as a TPC Member for many IEEE conferences, such as Globecom, ICC, and WCNC. He is also an Editor of IEEE COMMUNICATIONS LETTERS, IET Communications, and Frontiers in Signal Processing. He has served as a Guest Editor for several journals, such as IEEE INTERNET OF THINGS JOURNAL and Journal of Communications and Networks.

Boya Di (Member, IEEE) received the B.S. degree in electronic engineering from Peking University, Beijing, China, in 2014, and the Ph.D. degree from the Department of Electronics, Peking University, in 2019.

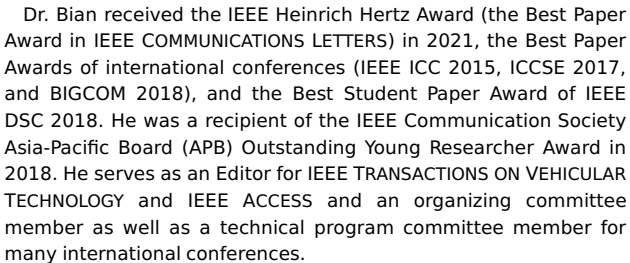
She was a Postdoctoral Researcher at Imperial College London, London, U.K. She is currently an Assistant Professor with Peking University. Her current research interests

University. Her current research interests include reconfigurable intelligent surfaces, multiagent systems, edge computing, vehicular networks, and aerial access networks.

Dr. Di received the Best Doctoral Thesis Award from the China Education Society of Electronics in 2019. She was a recipient of the 2021 IEEE ComSoc Asia-Pacific Outstanding Paper Award. She serves as an Associate Editor for IEEE TRANSACTIONS ON VEHICULAR TECHNOLOGY since June 2020. She has served as the Workshop Co-Chair for IEEE WCNC 2020&2021.

Kaigui Bian (Senior Member, IEEE) received the B.S. degree in computer science from Peking University, Beijing, China, in 2005, and the Ph.D. degree in computer engineering from Virginia Tech, Blacksburg, VA, USA, in 2011.

He was a Visiting Young Faculty Member with Microsoft Research Asia, Beijing in 2013. His research interests include wireless networking and mobile computing.



Zhu Han (Fellow, IEEE) received the B.S. degree in electronic engineering from Tsinghua University, Beijing, China, in 1997, and the M.S. and Ph.D. degrees in electrical and computer engineering from the University of Maryland, College Park, MD, USA, in 1999 and 2003, respectively.

From 2000 to 2002, he was a Research and Development Engineer with JDSU, Ger-

and Development Engineer With JDSU, Germantown, MD, USA. From 2003 to 2006, he was a Research Associate with the University of Maryland. From 2006 to 2008, he
was an Assistant Professor with Boise State University, Boise, ID,
USA. He is currently a John and Rebecca Moores Professor with
the Department of Electrical and Computer Engineering and the
Department of Computer Science, University of Houston, Houston,
TX, USA. His research interests include wireless resource allocation
and management, wireless communications and networking, game
theory, big data analysis, security, and smart grid.

Dr. Han has been a Fellow of AAAS since 2019 and a Distinguished Member of ACM since 2019. He received the NSF Career Award in 2010, the Fred W. Ellersick Prize of the IEEE Communication Society in 2011, the EURASIP Best Paper Award for the EURASIP Journal on Advances in Signal Processing in 2015, IEEE



Leonard G. Abraham Prize in the field of communications systems (the Best Paper Award in IEEE JOURNAL ON SELECTED AREAS IN COMMUNICATIONS) in 2016, and several best paper awards in IEEE conferences. He is also the winner of the 2021 IEEE Kiyo Tomiyasu Award, for outstanding early to mid-career contributions to technologies holding the promise of innovative applications, with the following citation: "for contributions to game theory and distributed management of autonomous communication networks." He was a Distinguished Lecturer of IEEE Communications Society from 2015 to 2018. He has been a 1% highly cited researcher since 2017 according to Web of Science.

H. Vincent Poor (Life Fellow, IEEE) received the Ph.D. degree in electrical engineering and computer science from Princeton University, Princeton, NJ, USA, in 1977.

From 1977 until 1990, he was on the faculty of the University of Illinois at Urbana-Champaign, Urbana, IL, USA. Since 1990, he has been on the faculty at Princeton, where he is currently the Michael Henry Strater



University Professor. From 2006 to 2016, he served as the Dean of Princeton's School of Engineering and Applied Science. He has also held visiting appointments at several other universities, including most recently at Berkeley and Cambridge. His research interests are in the areas of information theory, machine learning and network science, and their applications in wireless networks, energy systems, and related fields. Among his publications in these areas is the forthcoming book *Machine Learning and Wireless Communications* (Cambridge University Press).

Dr. Poor is a member of the National Academy of Engineering and the National Academy of Sciences and is a foreign member of the Chinese Academy of Sciences, the Royal Society, and other national and international academies. He received the IEEE Alexander Graham Bell Medal in 2017.

Lingyang Song (Fellow, IEEE) received the Ph.D. degree from the University of York, York, U.K., in 2007.

He worked as a Postdoctoral Research Fellow with the University of Oslo, Oslo, Norway, and Harvard University, Cambridge, MA, USA, until rejoining Philips Research, Cambridge, U.K., in March 2008. In May 2009, he joined the School of



Electronics Engineering and Computer Science, Peking University, Beijing, China, as a Full Professor. His main research interests include cooperative and cognitive communications, physical layer security, and wireless ad hoc/sensor networks. He has published extensively, wrote six text books, and is the co-inventor of a number of patents (standard contributions).

Dr. Song received nine paper awards in IEEE journals and conferences, including IEEE JSAC 2016, IEEE WCNC 2012, ICC 2014, Globecom 2014, and ICC 2015. He is currently on the Editorial Board of IEEE TRANSACTIONS ON COMMUNICATIONS and Journal of Network and Computer Applications. He served as the TPC Co-Chair for ICUFN from 2011 to 2012 and the symposium Co-Chair for IWCMC from 2009 to 2010, IEEE ICCT in 2011, and IEEE ICC from 2014 to 2015. He received the K. M. Stott Prize for excellent research from the University of York. He was a recipient of the 2012 IEEE Asia Pacific (AP) Young Researcher Award. He has been a Distinguished Lecturer of IEEE Communications Society since 2015.